UCRL-10242

University of California

Ernest O. Lawrence Radiation Laboratory

TWO-WEEK LOAN COPY

This is a Library Circulating Copy which may be borrowed for two weeks. For a personal retention copy, call Tech. Info. Division, Ext. 5545

Berkeley, California

DISCLAIMER

This document was prepared as an account of work sponsored by the United States Government. While this document is believed to contain correct information, neither the United States Government nor any agency thereof, nor the Regents of the University of California, nor any of their employees, makes any warranty, express or implied, or assumes any legal responsibility for the accuracy, completeness, or usefulness of any information, apparatus, product, or process disclosed, or represents that its use would not infringe privately owned rights. Reference herein to any specific commercial product, process, or service by its trade name, trademark, manufacturer, or otherwise, does not necessarily constitute or imply its endorsement, recommendation, or favoring by the United States Government or any agency thereof, or the Regents of the University of California. The views and opinions of authors expressed herein do not necessarily state or reflect those of the United States Government or any agency thereof or the Regents of the University of California.

Submitted to Physical Review

UCRL-10242

UNIVERSITY OF CALIFORNIA
Lawrence Radiation Laboratory
Berkeley, California

Contract No. W-7405-eng-48

NUCLEAR ALIGNMENT OF Ce^{137m}, Ce^{137}, Ce^{139}, Ce^{141}, and Ce^{143}

J. N. Haag, D. A. Shirley, and David H. Templeton

NUCLEAR ALIGNMENT OF Ce^{137m}, Ce^{137}, Ce^{139}, Ce^{141}, and Ce^{143}

J. N. Haag, D. A. Shirley, and David H. Templeton

Lawrence Radiation Laboratory and Department of Chemistry
University of California, Berkeley, California

ABSTRACT

Nuclei of Ce^{137m}, Ce^{137}, Ce^{139}, Ce^{141}, and Ce^{143} were aligned at low temperatures by the magnetic hyperfine-structure method. The angular distributions and the plane polarization of the emitted gamma radiation were measured as functions of temperature. For the spin sequence (Ce^{137m}) 11/2 (M4, E5, 255 keV) 3/2 (Ce^{137}), the mixing ratio, $|\delta(E5/M4)|$ is less than 0.7. For the sequence (Ce^{137}) 3/2 (i_β = 0,1) 3/2 (M1, E2, 445 keV) 5/2, the magnetic moment of Ce^{137} is $|\mu_N| = 0.90 \pm 0.15$ nm and $-2.6 < \delta(E2/M1) < -0.17$. The spin of the 455 keV level of La^{137} is shown to be 3/2. For the sequence (Ce^{139}) 3/2 (i_β = 1) 5/2 (M1, E2, 166 keV) 7/2 (La^{139}), the magnetic moment of Ce^{139} is $|\mu_N| = 0.95 \pm .20$ nm and $\delta(E2/M1) = +0.034 \pm .034$. The 166 keV level of La^{139} has spin 5/2. For the sequence (Ce^{141}) 7/2 (i_β = 0) 7/2 (M1, E2, 142 keV) 5/2 (Pr^{141}), the magnetic moment of Ce^{141} is $\mu_N = 1.30 \pm .20$ nm and $\delta(E2/M1) = +0.066 \pm .022$. The spin of the 142-keV level of Pr^{141} is established as 7/2. The beta transition is predominantly $i_\beta = 0$. For the sequence 7/2 (Ce^{143}) (i_β = 0, 1) 5/2 (7/2) (M1, E2, 294 keV) 5/2 (7/2), the magnetic moment of Ce^{143} is $|\mu_N| = 1.0 \pm 0.3$ nm, and $\delta(E2/M1) = -0.80 \pm .20$. The magnetic moments were found to be in agreement with configuration-mixing calculations. Evidence was found for two kinds of orientation attenuation in cerium magnesium nitrate.

NUCLEAR ALIGNMENT OF Ce^{137m}, Ce^{137}, Ce^{139}, Ce^{141}, and Ce^{143}*

J. N. Haag,† D. A. Shirley, and David H. Templeton

Lawrence Radiation Laboratory and Department of Chemistry
University of California, Berkeley, California

May, 1962

1. INTRODUCTION

The magnetic dipole moments of near-spherical nuclei deviate from the theoretical shell-model values.[1] In order to obtain additional systematic data on this phenomenon, the magnetic moments of Ce^{137}, Ce^{139}, Ce^{141}, and Ce^{143} were measured. The determination of the magnetic moment of Ce^{137m} has already been reported.[2]

The atomic-beam technique of determining magnetic moments has to date proven unsuccessful for cerium.[3] Paramagnetic resonance methods have been used to determine the magnetic moment[4] only of Ce^{141}. However, by use of the low-temperature magnetic hyperfine-structure method of nuclear alignment, magnetic moments were determined for the four isotopes above. In addition, information was obtained on the angular momenta and the mixing ratios in the decay of these four isotopes and in the decay of Ce^{137m}. Finally, a measure of the validity of the nuclear alignment results for cerium was obtained by comparing the alignment result for the magnetic moment of Ce^{141} with the result determined from paramagnetic resonance.

2. EXPERIMENTAL PROCEDURE

The nuclear reactions used to produce the various cerium radioisotopes studied are given in Table I.

Table I. Nuclear reactions for producing Ce radioisotopes.

Isotope	Reaction	Target
Ce^{137}	La^{139} (p, 3n) Ce^{137}	La metal
Ce^{137m}	La^{139} (p, 3n) Ce^{137m}	La metal
Ce^{139}	La^{139} (p, n) Ce^{139}	La metal
Ce^{141}	Ce^{140} (n, γ) Ce^{141}	Ce_2O_3 powder
Ce^{143}	Ce^{142} (n, γ) Ce^{143}	CeO_2 powder (90% Ce^{142})

In each case cerium was separated from the target material by oxidation to the +4 state, followed by solvent extraction.[5] The cerium was then reduced to the +3 state and grown either into a single crystal of neodymium ethylsulfate nonahydrate $Nd(C_2H_5SO_4)_3 \cdot 9H_2O$, (NES) so that it replaced some of the Nd^{+3} ions or into a cerium magnesium nitrate, $Ce_2Mg_3(NO_3)_{12} \cdot 24H_2O$, (CMN) crystal. The crystal was mounted in a demagnetization cryostat. Previous experiments[6,7] had shown that nuclear alignment of cerium nuclei can be produced by cooling such a crystal to very low temperatures.

The crystal was cooled by adiabatic demagnetization from 1.2°K and fields of up to 18,000 gauss. The magnetic temperature T^* of the crystal after demagnetization was determined by measuring the mutual inductance of a pair of coils surrounding the crystal, using a 20-cycle/sec ac mutual-inductance bridge. The coils were calibrated in the liquid helium range from 4.2- to 1.2°K against a helium vapor-pressure thermometer. From the data of Meyer,[8] and of Daniels and Robinson[9] the absolute temperatures T reached immediately after an adiabatic demagnetization from an initial

temperature $T_i = 1.2^{\circ}K$, and various initial fields H_i, were known. A correlation between T and T^* was determined by extrapolating our measured value of T^* to the time of demagnetization.

The time taken for the temperature of the crystal to rise from the lowest temperature reached ($0.02^{\circ}K$) to that of the helium bath ($1.2^{\circ}K$) was was over five hours for NES and one hour for CMN. Nevertheless, in order to avoid errors from inhomogeneous heating of the crystal, the gamma-ray intensity measurements were continued for not more than six minutes and the gamma-ray polarization measurements were continued for not more than 20 minutes. The crystal was then warmed to $1.2^{\circ}K$ by the introduction of helium exchange gas. Another gamma-ray measurement of appropriate duration was then taken for normalization. The intensity and plane polarization of the gamma radiation were isotropic within experimental error at this temperature.

The intensity of the gamma radiation was measured at several temperatures between 0.02- and $1.2^{\circ}K$ for a series of angles θ, defined by the direction of propagation of the gamma radiation with respect to the trigonal axis of the crystal. The gamma rays were counted using 3- × 3-in. NaI(Tl) crystals and 100-channel pulse-height analyzers. Each intensity measurement was corrected for background and the finite counter size effect,[10] as well as gain shift, block time, and decay. The total correction was always a small fraction of the observed anisotropy.

The plane polarization of the gamma radiation was measured for several temperatures between 0.02- and $1.2^{\circ}K$ at $\theta = 90$ deg., where the polarization had its maximum value. The gamma-ray polarimeter, utilizing Compton-scattering as the analyzing process, was similar to those described in the literature.[11,12] The gamma radiation emitted at $\theta = 90$ deg. was Compton-scattered from a 1.5- × 1.5-in. cylindrical anthracene crystal into one of two mutually

perpendicular 1- × 1.5-in. NaI(Tl) crystals. The mean angle of scattering, δ, was 80°. A "fast-slow" coincidence circuit with a resolving time of 2×10^{-9} second was utilized to measure coincidence events between the anthracene crystal and either of the two NaI crystals.

Because the three crystals were finite, a 0.5-curie source of Co^{60} was used to measure the geometry correction factor R of this polarimeter. This factor, the count ratio corresponding to complete polarization, is a function both of the energy of the quanta impinging on the anthracene crystal and of the geometry of the polarimeter. Using both the 1.17- and 1.33-MeV gamma rays of Co^{60}, a value of $R = 2.8 \begin{smallmatrix} +0.4 \\ -0.3 \end{smallmatrix}$ was found. Utilizing this value and the integral Klein-Nishina Compton-scattering cross section formula,[13] a geometric spread corresponding to $\Delta\delta = \Delta\eta = 70 \pm 7$ deg. was obtained. Here η is the angle between the direction of polarization (electric field vector direction) of the incident quantum and the plane of scattering. This result compared favorably with the geometrically calculated one of $\Delta\delta = \Delta\eta =$ 66 deg. This calculation assumed that all quanta were scattered at the geometric center of the anthracene crystal. With the experimental value $\Delta\delta = \Delta\eta = 70$ deg., the three curves in Fig. 1 were calculated.

3. THEORY OF THE MEASUREMENTS

The angular distribution of gamma radiation from aligned nuclei is given[12] by

$$I(\theta) = \sum_k B_k U_k F_k' P_k(\cos\theta) \qquad (1)$$

the factors B_k are a measure of the degree of orientation of the parent nucleus. The factors U_k describe the amount of nuclear re-orientation that

takes place during any preceeding unobserved beta or gamma transition. The factors F_k are functions determined by, for pure transitions, the multipolarity and the initial and final spins of the observed gamma transition; for mixed transitions involving multipolarities L and L', the functions are also determined by the amplitude mixing ratio $\delta(L'L)$. The functions $P_k(\cos\theta)$ are Legendre polynomials of order k, where k is an even interger.

If the plane polarization of gamma radiation is observed, Eq. (1) becomes[12,14]

$$I(\theta,\phi) = \sum_k B_k U_k [F_k' P_k (\cos\theta) + \cos(2\phi) F_k'' P_k^{(2)} (\cos\theta)] \qquad (2)$$

The factors F_k'' are functions of the electric or magnetic character of the observed gamma transition and of the same quantities which determine the F_k'. The quantity ϕ is the angle between the electric field vector of the polarized quantum and the plane containing the axis of orientation and the initial direction of propagation of the observed quantum. The functions $P_k^{(2)}(\cos\theta)$ are associated Legendre polynomials. In our work the $k > 4$ terms are negligible. Therefore Eq. (1) can be written as

$$I(\theta) = 1 + B_2U_2F_2'P_2 + B_4U_4F_4'P_4 . \qquad (3)$$

Substituting $\theta = 90$ deg. (the angle at which the polarimeter was placed because the polarization effect is largest there) and $\phi = 0$ deg. and $\phi = 90$ deg. (the angles at which the two NaI crystals were located in the polarimeter), Eq. (2) may be used to define the polarization p:

$$p = \frac{I(90^\circ,0^\circ)}{I(90^\circ,90^\circ)} = \frac{1 + B_2U_2(-1/2F_2' + 3F_2'') + B_4U_4(3/8\ F_4' - 15/2\ F_4'')}{1 + B_2U_2(-1/2F_2' - 3F_2'') + B_4U_4(3/8\ F_4' + 15/2\ F_4'')}$$

$$= \frac{R-N}{NR-1} \qquad (4)$$

The geometry correction factor R is the ratio of two incremental Klein-Nishina Compton-scattering cross sections.[13] For "ideal" geometry, R is $d\sigma\ (90^\circ)/d\sigma\ (0^\circ)$, where

$$d\sigma(\eta) = (r_0^2/2)\ d\Omega\alpha^2/\alpha_0^2\ (\alpha/\alpha_0 - \alpha_0/\alpha - 2\sin^2\delta\cos^2\eta).$$

Here $r_0 = e^2/mc^2)$ is the classical radius of the electron of mass m and charge e, c is the velocity of light, $d\Omega$ is the element of solid angle, α_0 is the energy of the incident quantum in units of mc^2, and the energy of the scattered quantum in units of mc^2 is

$$\alpha = \alpha_0/[1 + \alpha_0\ (1 - \cos\delta)\ ].$$

The ratio $N = N_{\parallel}/N_{\perp}$ was measured experimentally. Here $N_{\parallel}$ is the intensity of quanta scattered by the anthracene crystal into the detector in the plane containing the axis of orientation and the initial direction of propagation of the quanta ($\theta = 90^\circ$), and $N_{\perp}$ is the intensity of quanta scattered into the other detector.

4. THE SPIN-HAMILTONIAN

The crystal-field theory of Ce^{+3} in the ethylsulfate nonahydrate lattice has been worked out in detail by Elliott and Stevens,[15,16] and only

a brief account will be given here. The free ion Ce^{+3} has the configuration $4f^1$ and the ground level $^2F_{5/2}$. In a trigonal crystalline field this term is split into doublets which may be characterized in the first approximation by $|\pm J_z\rangle$. In the ethylsulfate lattice, however, the lowest Kramers' doublet, which is made mostly of the state $|\pm 5/2\rangle$, contains in addition admixtures of other states from the $^2F_{5/2}$ ground level as well as from the next level $^2F_{7/2}$. It is, of course, essential that these admixtures be taken into account in calculating the nuclear magnetic moment from hyperfine-structure constants.

The effective spin-Hamiltonian for the lowest Kramers' doublet of cerium in the ethylsulfate lattice is

$$\mathcal{H} = AS_zI_z + B(S_xI_x + S_yI_y) + P\,[I_z^2 - 1/3\ I\ (I+1)] \qquad (5)$$

By use of the theory of Elliott and Stevens for the ground doublet, together with the value of $\langle r^{-3}\rangle$, where r is the radius of the 4f electron orbital of Ce^{+3}, obtained by Judd and Lindgren,[17] we calculate

$$A = 0.074\ \mu_N/I\ \mathrm{cm}^{-1},\ B/A = 1/43.5,\ P/A \approx \frac{0.2}{2I - 1}\left(\frac{Q}{\mu_N}\right)$$

where μ_N is the nuclear magnetic dipole moment, I is the angular momentum of the aligned cerium nucleus, and Q is its nuclear electric quadrupole moment. The parameter B alters the energy levels of the hyperfine-structure multiplet slightly. However, our calculations showed that the small effect of this alteration was well within the statistical error of the experimental measurements, and the B term was neglected. Calculations based on the nuclear shell model[18] indicated that $|Q|$ should be of the order

of 0.5 barns or less for all these cerium nuclei, yielding a P always less than 4% of A. Thus the term in P should have negligible effect on alignment of the cerium nuclei; in fact these experiments showed no effects due to this P term.

Thus the Hamiltonian which was actually used in interpreting the ethylsulfate experiments was $\mathcal{H} = AS_z I_z$. In the CMN lattice the zero field spin-Hamiltonian is[4] $\mathcal{H} = B(S_x I_x + S_y I_y)$, and the alignment is planar rather than axial. Kedzie, et al. have found for Ce^{141} $B = 0.0126\ cm^{-1}$, from which, using the new values[17] for $\langle r^{-3} \rangle$, we obtain $\mu_N = 1.17$ n.m. For any cerium isotope in this lattice, then,

$$\mu_N = 26.5\ IB, \tag{6}$$

with μ_N in n.m. and B in cm^{-1}.

Nuclear alignment experiments give only the magnitude, and not the sign, of the hyperfine structure constant, and thus of the nuclear moment.

5. COMPUTATIONAL PROCEDURE

In the NES experiments we measured both the directional and the polarization anisotropies. Explicit procedures for the reduction of this type of data have not been given before in the literature. Because of the complexity which arises from γ-rays of mixed multipolarity we describe briefly a systematic data-reduction scheme. First we fitted a curve to the data which reproduced the temperature dependence. Then we eliminated the temperature variable in the following analysis by using only the values of $I(\theta)$ and P (obtained from the curve) at a given temperature, $T = 0.02^{\circ}K$.

If the measured $I(0^{\circ})$ was greater than 1, Eq. (3) gave

$$B_2U_2F_2' + B_4U_4F_4' > 0$$

therefore

$$F_2' > -\left(\frac{B_4U_4}{B_2U_2}\right) F_4' \equiv A'$$

Similarly, for $I(90^\circ)$ smaller than 1,

$$F_2' > 3/4 \left(\frac{B_4U_4}{B_2U_2}\right) F_4' \equiv B'$$

and for $p > 1$, Eq. (4) gave

$$F_2'' > 5/2 \frac{B_4U_4}{B_2U_2} F_4'' \equiv C'.$$

Extending this technique to all possible combinations of $I(0^\circ)$, $I(90^\circ)$, and p gives Table II.

In Table II, the subscript "min" or "max" indicates that A', B', and C' are to be evaluated at their <u>algebraic</u> minima or maxima. The limits calculated for δ by this technique are those that insure the correct sign for the quantities $I(90^\circ)$, $I(0^\circ)$, and p. The technique has been found in this work to excell "trial-and-error" methods, as it reveals all possible δ that may satisfy the experimental results and considerably restricts the allowable ranges of δ.

The directly measurable experimental quantities $I(\theta)$ and p are expressed explicitly in terms of δ and μ through functional relationships which cannot readily be inverted. The next step in reducing the data was thus to limit the <u>a priori</u> acceptable values of $|\mu_N|$ to a certain range.

Table II. Boundary conditions on δ

	$I(0^\circ)>1, I(90^\circ)<1$	$I(0^\circ)<1, I(90^\circ)>1$	$I(0^\circ)>1, I(90^\circ)>1$	$I(0^\circ)<1, I(90^\circ)<1$
	$F_2' > A'_{min}$	$F_2' < A'_{max}$	$F_2' > A'_{min}$	$F_2' < A'_{max}$
$p > 1$	$F_2' > B'_{min}$	$F_2' < B'_{max}$	$F_2' < B'_{max}$	$F_2' > B'_{min}$
	$F_2'' > C'_{min}$	$F_2'' > C'_{min}$	$F_2'' > C'_{min}$	$F_2'' > C'_{min}$
	$F_2' > A'_{min}$	$F_2' < A'_{max}$	$F_2' > A'_{min}$	$F_2' < A'_{max}$
$p < 1$	$F_2' > B'_{min}$	$F_2' < B'_{max}$	$F_2' < B'_{max}$	$F_2' > B'_{min}$
	$F_2'' < C'_{max}$	$F_2'' < C'_{max}$	$F_2'' < C'_{max}$	$F_2'' < C'_{max}$

For these odd-neutron nuclei this range may conveniently be taken as between 0 and the magnitude of the Schmidt limit (it can subsequently be shown separately in each case that no value of $|\mu_N|$ outside the Schmidt limit would reproduce the experimental temperature dependence of anisotropy). A nonzero lower limit on $|\mu_N|$ is obtained by comparing the maximum allowable F_2 with the data at $T = .02^{\circ}K$

The acceptable ranges of μ_N and δ allowed by the above criteria may be further restricted, next, by requiring that δ and $|\mu_N|$ fit the $0.02^{\circ}K$ data simultaneously (i.e., solving for $\mu_N(\delta)$), and finally, by making a detailed quantitative comparison of the curves calculated from $\mu_N(\delta)$ with the experimental data, as a function of temperature. Thus one obtains, in general, sets of allowable ranges of $|\mu_N|$ and δ. There is no guarantee a priori that these ranges will be unique or narrow, but often other decay-scheme data can be invoked to further restrict δ.

6. EXPERIMENTAL RESULTS AND DERIVED QUANTITIES

For convenience each nuclide is discussed separately below, from the presentation of the data to a statement, where possible, of the derived μ_N and δ. For brevity we do not give a complete discussion of the decay scheme in each case, but rather cite references in which such information may be found.

Ce^{137m}

The decay scheme of this 34-hour isomer and the 9-hour isomer is given, for reference, in Figure 2.[19] In earlier nuclear alignment experiments[2] the magnetic moment of Ce^{137m} was found to be $|0.96 \pm 0.09|$nm and the spin

was shown to be 11/2. In the present work the linear polarization of the 255-keV γ-ray from Ce^{137m} oriented in NES was measured as a function of temperature, with the results shown in Figure 3. The theoretical curves are based on a pure M4 transition and the upper and lower limits, above, for $|\mu_N|$. The good agreement of experiment and theory confirms this $|\mu_N|$ value. Conversely, one can compare the value for $|\mu_N|$ derived independently (below) with the polarization data to confirm the M4 multipolarity assignment. It is readily established that $|\delta\ (\frac{E5}{M4})| < 0.7$. Of course one expects the E5 transition probability to be several orders of magnitude below the M4. We mention this result because it represents direct experimental evidence obtained by an unusual technique.

The crystal lattice cerium magnesium nitrate (CMN) has been used for nuclear orientation with varying success in the past. In particular very small magnetic moments could be derived from data on some isotopes oriented in CMN.[7,20] This type of result can arise because of a (possibly temperature-dependent) attenuation of the nuclear orientation. Such attenuation can be caused by spin-spin interactions or by perturbation in an intermediate state following decay of the parent. A low apparent magnetic moment can also arise from an incomplete knowledge of the absolute temperature, brought about by a large heat leak into the crystal and consequent rapid "warm up" rate. The main effect of this is to "wash out" the structure in the $I(\theta)$ vs $1/T$ curve, thus eliminating evidence of saturation of the nuclear orientation and making the nuclear moment appear to be smaller than it really is. This effect is especially important in the case of CMN because this salt has an extremely small magnetic heat capacity and is thus very difficult to keep cold. We have accumulated abundant (unpublished) experimental evidence for this effect in this laboratory in experiments which didn't work. We believe that it would

be very difficult to obtain reliable quantitative information from experiments with CMN in which the total "warm-up time" to the bath temperature was much less than 1 hour.

For Ce^{137m} in CMN there is no chance for perturbation in an intermediate state to affect the anisotropy, and this experiment should therefore provide some test of the hypothesis[20] that spin-spin interactions involving the cerium parent attenuate the orientation. All the odd cerium isotopes have magnetic moments in the neighborhood of 1.0 nm. It follows that the attenuation effect, which is closely related to the nuclear moment (rather than the spin), should be about the same for all these isotopes.

The temperature dependence of the intensity, at 0° and 90° from the c axis, of the 255-keV γ-ray from Ce^{137m} oriented in CMN is shown in Figure 4. In Figure 5 is plotted the angular distribution at $0.0043^{\circ}K$. A theoretical curve calculated with the aid of the Hamiltonian $\mathcal{H} = B(S_x I_x + S_y I_y)$, which is appropriate for Ce^{+3} in a CMN lattice, with $B = 0.0063\ cm^{-1}$, is shown in Fig. 4. This corresponds to a nuclear moment of 0.92 nm. which is within the limits of error of the experimental value.[2] This value of μ_N gives the best fit available, but it is not possible to fit the data very well with this Hamiltonian. We have some reservations about the quality of these data, particularly with respect to the temperature scale, which may be in error by a few percent for this particular crystal. We feel that the experiment should be repeated before a quantitative interpretation of the apparently anomalous temperature dependence is worthwhile. We can conclude, however, (1) the theoretical curve gives a fair fit to the data using the above simple Hamiltonian and the known magnetic moment of Ce^{137m}. If the moment were unknown one might derive a moment of $|\mu_N| = 0.92 \pm 0.15$ nm from the data. Thus it seems unlikely that interactions in the parent ions could substantially

affect the derived moments for cerium isotopes in CMN, and (2) even allowing for a possible substantial systematic experimental error it seems unlikely that the above Hamiltonian is completely adequate, and there is considerable evidence for a temperature-dependent effect (on the nuclear orientation) which is, however, much smaller than was previously indicated.[20]

Ce^{137}

Because the half life of Ce^{137} (9 hr) is long compared with the (nuclear) spin-lattice relaxation time, the anisotropy of its γ radiation does not depend on the preceding isomeric transition of Ce^{137m}. A source was prepared with five times the activity of the source used in the Ce^{137m} experiment. The 166-keV γ ray of La^{139} and the 255 keV γ ray of Ce^{137m} were discriminated off the pulse-height analyzer so that only the 445-keV γ ray of La^{137} was counted. The experiment was started 200 hr after the bombardment and decay corrections were based on the transient equilibrium half life of 34 hr, the half life of Ce^{137m}.

The intensity of the 445-keV γray of La^{137} as a function of 1/T is shown in Fig. 6 for NES and in Fig. 7 for CMN. The angular distribution in NES at $0.02^{\circ}K$ was found to be

$$I(\theta) = 1 - (0.060 \pm .010)\, P_2(\cos\theta). \qquad (7)$$

A $P_4(\cos\theta)$ term was not indicated by the data. This term theoretically vanishes if the ground-state spin of Ce^{137} is 3/2.

For the 445-keV transition of La^{137}, the unobserved preceding β transition gives, for the sequence $3/2 \xrightarrow{i_\beta} 3/2$, $U_2 = 1.000$ for a pure $i_\beta = 0$ transition and $U_2 = 0.2000$ for a pure $i_\beta = 1$ transition. Of course any mixture of $i_\beta = 0$ and 1 is allowed, and the range of U_2

is thus 0.2 - 1.0. In order to determine the multipolarity accurately, it would be necessary to determine F_2 accurately independently of U_2, using polarization measurements. Although we took some 23 experimental polarization points using NES, the statistical scatter was large enough to preclude using these data to narrow the multipolarity range on the 445-keV γ-ray, and we can say only that, at $0.02^{\circ}K$, $p \sim +1.5$.

From the sign of the anisotropy we can immediately infer that $-0.08 > \delta(445) > -3.5$. From the magnitude of U_2F_2 (established below) we can reduce the allowable range further to $-0.17 > \delta(445) > -2.6$.

The saturation behavior of the orientation of Ce^{137} in CMN allows us to set a useful lower limit on $|\mu_N|$. Any smaller nuclear moment would not reproduce the saturation behavior satisfactorily. In fact it is easily shown that β ($\equiv B/2kT$ in this case) must be greater than 1.6 at $0.01^{\circ}K$. It follows that $B \geq 0.022\ cm^{-1}$ or, using Eq. (6), that $|\mu_N| \geq 0.85$ nm. Similarly it is possible, for $U_2 F_2$, to set limits $-0.09 \geq U_2 F_2 \geq -0.12$. Comparing this range of $U_2 F_2$ with the experimental value $B_2 U_2 F_2 = -0.060 \pm 0.010$ from Eq. (7), we obtain $B_2(.02^{\circ}K) = 0.57 \pm 0.13$ for Ce^{137} in NES. It follows that, for this lattice, $A = 0.041\ cm^{-1}$. From Section 3 we find $|\mu_N| = 0.84 \pm^{0.20}_{0.14}$ nm. The allowed range overlaps considerably with that from the CMN data. Combining all the data, we obtain a weighted average of $|\mu_N| = 0.90 \pm 0.15$ nm.

As discussed before[2] our data rule out a spin of 1/2 for the 455 keV state in La^{137} because a nonzero anisotropy was observed. The state is assigned positive parity because the 445 keV transition is known to have M1-E2 multipolarity.[21] It seems unlikely that the spin of this state could be 5/2 on the basis of the absence of a crossover transition to the 7/2+ ground state.[21] Thus we conclude that the 455-keV state has character 3/2+ and that

the 445 keV γ-ray is of mixed M1-E2 multipolarity.

We have implicitly assumed above that there is no overall attenuation in the 455 keV γ-ray anisotropy. This is reasonable in view of the fact that there is no evidence that the 455-keV level of La^{137} is delayed. Because the transition probability for an M1 γ-ray has an E^3 dependence,[22] one can estimate from nuclear systematics that this state will have a lifetime $\tau < 10^{-10}$ sec, and no perturbations should occur in this time.

Ce^{139}

The decay schemes of Ce^{139m} and Ce^{139} have been studied by Ketelle, Thomas, and Brosi[23] utilizing γ-ray, coincidence, and conversion-electron spectroscopic techniques. Their results indicate the energy-level scheme shown in Fig. 8.

A $g_{7/2}$ orbital was assigned to the ground state of La^{139} on the basis of its measured spin[24] of 7/2. The 166-keV level was assigned a $d_{5/2}$ orbital from the M1 character of its γ ray and from its measured lifetime[25] of $1.5 \pm .1 \times 10^{-9}$ sec. The conversion-electron measurements by Dzhelepov et al.,[26] the Ce^{139m} half-life and energy measurements by Kotajima and Morinaga[27] and the Ba^{139}-to-La^{139} β-transition measurements by Kelly, et al.,[28] are all consistent with these assignments. The shell model is in complete agreement with these assignments, which are analogous to those for Ce^{137m}, Ce^{137}, and La^{137}.

The source used for this experiment was the same as that for the Ce^{137} experiment. After the source had decayed for 30 days, neither the 255-keV Ce^{137m} activity nor the 445-keV Ce^{137} activity was observable. The resulting γ-ray pulse-height spectrum obtained in this experiment is shown in Fig. 9. Only the 166-keV γ ray of La^{139} was present.

The intensity of the 166-keV γ ray of La^{139} as a function of $1/T$ is shown in Fig. 10 for NES and in Fig. 11 for CMN. The intensity $I(\theta)$ as a function of $P_2(\cos\theta)$ in NES at $1/T = 50$ is shown in Fig. 12. This angular distribution was found to be

$$I(\theta) = 1 + (0.080 \pm 0.008)\, P_2\,(\cos\theta). \tag{8}$$

A $P_4\,(\cos\theta)$ term was not indicated by the data. This term would vanish if the ground-state spin of Ce^{139} is 3/2.

For the 166-keV transition of La^{139}, the unobserved preceding (allowed) β transition for the sequence $3/2\ (i_\beta)\ 5/2\ (M1, E2)\ 7/2$ must have $i_\beta = 1$ and $U_2 = 0.7486$. Thus Eq. (3) becomes

$$I(\theta) = 1 + 0.7486 F_2'\,(1, 7/2, 5/2)\, B_2 P_2\,(\cos\theta), \tag{9}$$

and Eq. (4) becomes

$$p = \frac{1 + 0.7486 B_2\,[(-1/2)F_2'\,(1,7/2,5/2) + 3F_2''\,(1,7/2,5/2)]}{1 + 0.7486 B_2\,[(-1/2)F_2'\,(1,7/2,5/2) - 3F_2''\,(1,7/2,5/2)]} \tag{10}$$

Directional and polarization anisotropies were observed using NES. Only directional anisotropies were determined with CMN. The NES results are discussed first.

The value of p as a function of $1/T$ is shown in Fig. 13. The boundary conditions on δ were found as described before, yielding (since $B_4 = 0$)

$$F_2' > 0 \qquad \text{and} \qquad F_2'' > 0$$

Utilizing Fig. 14, four ranges for were found: $-4 > \delta > -\infty$, $0 > \delta > -0.1$, $0.7 > \delta > 0$, and $\infty > \delta > 1$.

Performing the calculations with Eq. 9 and 10, one could use the values of δ in the range -4 to $-\infty$ with various values for $|\mu_N|$ to reproduce the $I(0^\circ)$-vs-1/T curve. However, the resulting p-vs-1/T curve was consistently below the experimental curve. The values of in the range 0 to -0.1 could not be used to reproduce either the $I(0^\circ)$-vs-1/T or the p-vs-1/T curves. Some of the values of δ in the range 0.7 to 0 led to B_2, F_2', and F_2'' which reproduced both the experimental $I(0^\circ)$ curve and, except for one value, the p curve. The results are

$$|\mu_N| = 0.95 \pm 0.20 \qquad \delta = 0.034 \pm .034.$$

The limits of error were obtained as mentioned previously. Equation (8), the experimental angular distribution, is in agreement with these values.

The lowest-temperature value of p, Fig. 13, does not fall within the calculated limits. This experiment value for p, statistically speaking, can assume a broader range of values than any value for p at a lower 1/T. This is because the statistical counting error involved in measuring N has a greater effect on the total error in p (not shown in Fig. 13) as N deviates further from unity. In fact, the total error of this highest -1/T experimental value for p does just include the upper theoretical curve (solid line) of Fig. 13.

For the range $\infty > \delta > 1$, the results obtained are

$$|\mu_N| = 0.60 \pm .10, \qquad \infty > \delta > 40.$$

Figure 10 shows the resulting $I(0^{\circ})$-vs-1/T curve for $|\mu_N| = 0.60$ and $\delta = \infty$. Figure 13 shows the corresponding p-vs-1/T curve. We cannot rule out this combination of μ_N and δ from our data. Both Coulomb excitation experiments (which showed no 166-keV γ-ray)[29] and recent high-precision conversion electron data,[30] however, indicate that the transition is predominantly M1, and thus rule out this latter combination.

Spin sequences other than 3/2 (i_β) 5/2 (M1, E2) 7/2 may easily be ruled out. The anisotropy of the 166-keV γ ray excludes a spin 1/2 for either the Ce^{139} ground state or the 166-keV level of La^{139}. The sign of the observed anisotropy excludes the sequence 3/2 (i_β) 3/2 (E2) 7/2 as $F_2(2,2,7/2,3/2) = -0.1429$ and $U_2 > 0$. The log ft value for EC decay of Ce^{139} is not consistent with the sequence 3/2(i_β) 7/2 (M1, E2) 7/2.

The results for Ce^{139} in CMN are in fair agreement with these conclusions. A theoretical curve may be fitted to these data (Fig. 11)to give the hyperfine structure constant $B = 0.017 \pm 0.004\ cm^{-1}$. Comparison with Eq. (6) yields $|\mu_N| = .68 \pm .14$ nm. The hyperfine structure was large enough to allow partial saturation of the nuclear orientation in this lattice. Thus there is some structure in the curve in Fig. 11, and it is possible to derive the anisotropy coefficient, $G_2U_2F_2 = +0.106 \pm 0.011$, independently, from the directional anisotropy alone. We have written the attenuation factor G_2, familiar from angular correlation theory, in anticipation of our interpretation. It is possible that some attenuation of the orientation takes place in the 1.5 nsec 166 keV state in La^{139} in the CMN lattice. If so, the effect would be observable in a lower value of U_2F_2 derived from this experiment than from the NES experiment, where no attenuation is expected.[12] This apparent U_2F_2 can be termed $G_2U_2F_2$, which can then be compared with the known U_2F_2 from the NES experiment to give G_2. Unfortunately U_2F_2 was not determined

accurately in the NES experiment, because no appreciable saturation of the nuclear orientation was obtained. In fact the NES experiments yield a U_2F_2 in the range 0.10 to 0.17 and comparison gives $0.6 \leqslant G_2 \leqslant 1.0$.

A more precise value of G_2 may be obtained by requiring that the magnetic moment be the same in the two experiments. While this procedure is not without pitfalls, it seems worthwhile, if only to establish a most probable value for G_2. Assuming $\mu_N = 0.8$ nm we find $(U_2F_2)_{NES} = .148$, $(G_2U_2F_2)_{CMN} = .083$, and $G_2 = 0.56 \pm 0.10$. This value is derived from the CMN data at $0.01^{\circ}K$. It is likely that the effect is temperature-dependent. Our data are not accurate enough to permit a detailed discussion of this effect, especially considering that it is first necessary to separate the effects of spin-spin interactions, discussed under Ce^{137m}. It does seem possible to conclude that, in the CMN lattice, there is an overall attenuation of the nuclear orientation. This should be distinguished from Ce^{137m}, in which there was little overall attenuation in the CMN lattice, but the temperature dependence of the data could not be fitted by curves derived from the simple spin Hamiltonian. The precision available in these experiments was not sufficient to study attenuation effects properly, and our conclusions must be considered somewhat tentative. It would be interesting to study these effects much more carefully, and an experiment is being designed for this purpose.

In view of the (apparently temperature-dependent) attenuation present in CMN, we chose to give no weight to the magnetic moment derived therefrom, and we therefore adopt the values of μ_N and δ obtained from the NES data.

We note that our results for Ce^{139} in CMN are in reasonable agreement with the work of Ambler, et al.[20]

Ce^{141}

The decay scheme of Ce^{141} has been extensively studied by many authors. The results published prior to February, 1958, are summarized in the "Table of Isotopes".[31] More recent results, cited below, are consistent with previous ones and lead to the energy-level scheme shown in Fig. 15.

An $f_{7/2}$ orbital was assigned to the ground state of Ce^{141} on the basis of its measured spin of 7/2. The measured spin of 5/2 for the ground state of Pr^{141} lead to the assignment of a $d_{5/2}$ orbital to this state. The M1 character of the γ ray from the 142-keV level of Pr^{141} led to the assignment of a $g_{7/2}$ orbital to this level. The Nd^{141} to Pr^{141} β-decay measurements by Polak et al.[32] are consistent with these spin assignments. The K-conversion coefficients of Joshi et al.[33] and the $1.9 \pm .2 \times 10^{-9}$ -sec lifetime of the 142-keV level of Pr^{141}, as determined by DeWaard and Gerholm,[34] indicate an M1 character for this γ ray. That Heydenberg and Temmer[29] did not observe a 142-keV γ ray in Coulomb excitation work on Pr^{141} strongly indicates that the E2 admixture in this transition is small. The outstanding exception to all these conclusions on the M1 character of the 142-keV γ ray is the work of Cook.[35] He found $\alpha_K = 0.405 \pm .01$. This was interpreted as evidence of predominantly an E2 transition on the basis of his extrapolated curves for α_2 and β_1, based on the English edition of Sliv and Band's values.[36] Cook quoted his extrapolations as giving $\alpha_2 = 0.42$ and $\beta_1 = 0.435$. Using extrapolated curves[37] based on the same source, we found $\alpha_2 = 0.425 \pm .010$ and $\beta_1 = 0.405 \pm .010$. Comparing these values with Cook's experimental value for α_K gives the expected predominance of M1, not E2, character for the 142-keV γ ray.

The Ce^{141} source used for these experiments was allowed to decay for 30 days, so that the Ce^{143} activity would be absent from the γ-ray spectrum.

The resulting γ-ray pulse-height spectrum obtained then showed only the 142-keV activity. This spectrum is shown in Fig. 16 for $I(0^{\circ})$ and in Fig. 17 for $I(90^{\circ})$, in NES. In both figures, the change of intensity with temperature has opposite signs for the 142-keV peak and for the Compton distribution around 100 keV. This effect is due to the polarized γ ray's being Compton-scattered from the source crystal (15 grams of neodymium ethylsulfate) and from the glass walls of the apparatus. This phenomenon may prove to be more accurate means of determining the plane polarization of γ rays than the conventional polarimeter for energies less than about 500 keV. This is true because the counting rates are greater by orders of magnitude than with a polarimeter, no coincidence circuit being required. A quantitative expression for dealing with this effect is currently under preparation. The phenomenon holds promise for both nuclear alignment experiments and angular correlation experiments.

The intensity $I(0^{\circ})$ of the 142-keV γ ray of Pr^{141} as a function of $1/T$ is shown in Fig. 18. This angular distribution at $0.02^{\circ}K$ was found to be

$$I(\theta) = 1 + (0.170 \pm .006)\, P_2\, (\cos\theta). \qquad (11)$$

A $P_4\,(\cos\theta)$ term was not indicated by the data.

For the 142-keV transition of Pr^{141}, the unobserved preceding β transition for the sequence $7/2(i\beta)\ 7/2$ gives $U_2 = 1.000$ and $U_4 = 1.000$ for a pure $i_\beta = 0$ transition; for a pure $i_\beta = 1$ transition, $U_2 = 0.8096$ and $U_4 = 0.365$. On the assumption for the moment that $i_\beta = 0$, Eq. (3) becomes, for the spin sequence $7/2(0)\ 7/2\ (M1, E2)\ 5/2$.

$$I(\theta) = 1 + F_2'\ (1,5/2,7/2)B_2P_2(\cos\theta) + F_4'\ (1,5/2,7/2)B_4P_4(\cos\theta), \tag{12}$$

$$p = \frac{1 + B_2[(-1/2)F_2' + 3F_2''] + B_4\ [(3/8)F_4' - (15/2)F_4'']}{1 + B_2[(-1/2)F_2' + 3F_2''] + B_4\ [(3/8)F_4' + (15/2)F_4'']} \tag{13}$$

The value of p as a function of $1/T$ is shown in Fig. 19. Six measurements were made of N and used individually to calculate p vs $1/T$.

The boundary conditions on δ were found to be

$$F_2' > 0 \qquad \text{and} \qquad F_2'' > -0.039$$

for $|\mu_N| \leqslant 1.91$, the Schmidt limit (it was later found that a larger moment would require saturation of the nuclear orientation at a very high temperature, and wouldn't fit the data). By using Fig. 20, two ranges for δ was found: $0 > \delta > -0.7$ and $0.2 > \delta > 0$. No solution could be found for the first range. The small value for $|\mu_N|$ required for δ in this region gave a B_2 such that the $I(0^\circ)$-vs-$1/T$ curve of Fig. 18 could not be reproduced with regard to curvature as a function of $1/T$. In addition, the corresponding p-vs-$1/T$ curve always fell below the experimental curve.

The values of δ in the second range, using Eq. (12) and (13), which satisfied both the experimental $I(0^\circ)$ and p curves, gave

$$|\mu_N| = 1.30 \pm .20, \qquad \delta = +0.066 \pm .022.$$

Equation (11), the experimental angular distribution, agrees well with these values. No P_4 $(\cos\theta)$ term was seen experimentally, because of the small

$$F_4' = \frac{\delta^2}{1+\delta^2} F_4 (2,2,5/2,7/2) = 0.002.$$

The above results are based on the assumption that the beta transition is pure $i_\beta = 0$. For a pure $i_\beta = 1$ transition, Eq. (12) becomes

$$I(\theta) = 1 + 0.8096\, F_2'B_2P_2 (\cos\theta) + 0.365\, F_4'B_4P_4 (\cos\theta) ,$$

and Eq. (13) undergoes a corresponding change. The solution in this case is

$$|\mu_N| = 1.60 \pm .20 \qquad \delta = 0.66 \pm .022.$$

These values could not be used to reproduce the experimental $I(0^o)$ and p curves as well as in the case of the $i_\beta = 0$ solution. A moment this large introduces a curvature in B_2 as a function of $1/T$ that lies outside the statistical error of the measurements. Thus we conclude that the beta transition is predominantly $i_\beta = 0$. A more concrete indication is the measurement by Kedzie et al.[4] of the magnetic hyperfine coupling constant of Ce^{141} by paramagnetic resonance to give (when corrected to Judd and Lindgren's value for $\langle r^{-3}\rangle$)

$$|\mu_N| = 1.17 \pm 0.12.$$

This value is in good agreement with the value for $|\mu_N|$ found in our experiments for $i_\beta = 0$, and is independent of the beta transition involved in the decay of Ce^{141}. Therefore it can be concluded that the $7/2(i_\beta)7/2$ transition is predominantly an $i_\beta = 0$ beta transition.

Cacho et al.[6] obtained nuclear alignment results for Ce^{141} in a neodymium ethylsulfate lattice. Their findings (corrected to Judd and Lindgren's values[17] for $\langle r^{-3} \rangle$) were

$$|\mu_N| = 0.99 \pm .26 \text{ for } i_\beta = 1,$$

$$\delta = 0.08 \pm .02.$$

$$|\mu_N| = 0.87 \pm .21 \text{ for } i_\beta = 0$$

These results for $|\mu_N|$ are somewhat different from ours. This can be at least partially explained by the somewhat smaller anisotropies which they observed.

Spin sequences other than the $7/2(i_\beta)7/2$ (M1, E2)5/2 sequence used in interpreting our data seem highly improbable. The only spin involved in the decay that has not been measured is that of the 142-keV level of Pr^{141}. This cannot, on the basis of the anisotropy of the 142-keV γ ray, be spin 1/2. The experimental log ft values indicate a first-forbidden, I = 0 or 1, yes transition. Thus the spin is unlikely to be 3/2 or 11/2. The sign of the measured anisotropy definitely excludes a spin of 9/2, for this gives $U_2 > 0$, $U_4 > 0$ and $F_2(2,2,5/2,9/2) = -0.4325$, $F_4(2,2,5/2,9/2 = -0.2684$. The remaining possibility is a spin 5/2 for the 142-keV level. Evaluating the resulting boundary conditions for δ gives $F_2' > 0$ and $F_2'' > 0$. Two ranges in δ result from this. For the first range, $\infty > \delta > 5.6$ (thus predominantly an E2 transition), there is no solution for $|\mu_N| \leqslant 1.91$, the Schmidt limit, as in $F_2' \geqslant 0.24$ is required to reproduce the experimental $I(0^\circ)$ and p curves. However, the theoretical maximum for F_2' is 0.19.

For the second range $-2.5 > \delta > -\infty$ (predominantly an E2 transition), there also is no solution for $|\mu_N| \leqslant 1.91$. The experimental curve of $I(0^\circ)$ can be reproduced, but the p-vs-1/T curve cannot. The highest possible p value calculated from this range of δ is $p = 1.61$ at $1/T = 50$. Figure 19 shows that this value is completely outside our experimental values. Thus, we can uniquely assign a spin of 7/2 to the 142-keV level of Pr^{141}. The shell model is in agreement with this result.

Sapp and Strohm[38] have recently reported a nuclear alignment experiment on Ce^{141} in CMN in which they found an angular distribution $I(\theta) = 1 + A_2P_2(\cos\theta)$, with $A_2 = (+0.169\pm0.015)B_2$. After corrections this yields $G_2U_2F_2' = 0.174\pm0.015$. Using, for consistency, the magnetic moment of 1.17 nm which is obtained from the work of Kedzie et al[4], together with the calculations described in Sections 3 and 4, we may derive a value of 0.88 for B_2 in NES at 0.02°K. Comparison with Eq. (11) yields $U_2F_2' = +0.193\pm0.010$, in reasonable agreement with the above result. Thus G_2 is about unity in this case, and there is no evidence for attenuation in the CMN lattice.

Ce^{143}

The decay scheme of Ce^{143} was studied by Martin, et al.,[39] who found a prominent 294 keV γ-ray transition between states at 351 and 57 keV (Fig. 21). We have studied the directional and polarization anistropy of this γ-ray following the decay of Ce^{143} oriented in a crystal of NES. The results are shown in Figures 22 and 23.

The data available on the level scheme of Pr^{143} are far too incomplete to allow a unique interpretation of the nuclear alignment work. Nevertheless certain conclusions can be drawn.

The angular distribution of the 294-keV γ-ray at $0.02^{\circ}K$ is $I(\theta) = 1 + (0.045 \pm 0.010)P_2(\cos\theta)$, and at the same temperature $\cong 0.6$. From Eq. 4 it can easily be shown that the two results require $F_2' > 0$, $F_2'' \cong 2F_2'$. This combination is possible in a mixed M1-E2 transition only if the spins of the initial and final states are the same. In Fig. 24 the range of δ which fits these data for the spin sequence 7/2(M1, E2)7/2 is shown. Thus we may conclude that the 351 and 57-keV states have the same spin and that the 294-keV transition is mixed M1 and E2 with $\delta \cong -0.8$. These data further require that $\mu_N \approx 1$ for Ce^{143}.

On a more speculative level we might try to assign the spins of these excited levels of Pr^{143} as follows: States with spins 7/2+ and 5/2+ (mominally $g_{7/2}$ and $d_{5/2}$) occur in several nuclei in this region as the ground state and the first excited state. Because the ground state of Pr^{143} is known to have spin 7/2[40], it is reasonable to assign 5/2+ character to the 57-keV state. From the alignment data the 351-keV state would then also be 5/2+. The spin and parity of Ce^{143} is expected to be 7/2- from nuclear systematics.[39] If this assignment is correct the absence of β-decay to the ground state of Pr^{143} is very surprising.

DISCUSSION

Most of the results and conclusions are summarized in the abstract. It is interesting, however, to compare the magnetic moments of these cerium nuclei with theory. The appropriate theoretical model in this case is the nuclear shell model, modified to include configuration mixing, by Noya, Arima and Horie.[1] Using first-order perturbation theory and estimates of two-body interaction strengths determined from empirical data on pairing

energies, these authors have calculated the departure of magnetic dipole moments from the Schmidt limit due to configuration mixing between $j = \ell + 1/2$ and $j_1 = \ell - 1/2$ orbitals. On the basis of this model, they have calculated magnetic moments for about 100 near-closed shell nuclei. Their calculated results generally agree with experimental magnetic moments to within 0.3 nm. Table 3 shows a comparison betwen the $|\mu_N|$ (exp) from the nuclear alignment results and the μ_N (calc) for both the Schmidt limit and the configuration-mixing model.

The proton configurations given in this table represent those protons outside the $Z = 50$ closed shell. The zeroth-order neutron configurations given for Ce^{137m}, Ce^{137}, and Ce^{139} represent those neutrons outside the N=50 closed shell and the $1g_{7/2}$ closed subshell. The neutron configurations given for Ce^{139} and Ce^{141} represent those neutrons in the $1h_{11/2}$ subshell and those outside the $N = 82$ closed shell. The excitation mode of the neutron given in this table illustrates the configuration mixing between $j = \ell + 1/2$ and $j_1 = \ell - 1/2$ orbitals. The protons cannot be excited within the framework of this model because both the $1g_{9/2}$ and $1g_{7/2}$ subshells are filled. With the exception of Ce^{143}, only one mode of excitation is possible for the neutron configuration of each isotope. In Ce^{143}, two excitation modes are simultaneously possible: the $1h_{11/2} \longrightarrow 1h_{9/2}$ and $2f_{7/2} \longrightarrow 2f_{5/2}$ modes. The Schmidt limits, μ_N(calc), were calculated on the basis of the zeroth-order neutron configurations. The configuration-mixing model magnetic moments, μ_N(calc), were calculated on the basis of the excitation modes of the neutron for two values of C, the ratio of an experimental neutron pairing energy to the product of $(j+1/2)$ times $A^{-1/2}$ times a harmonic oscillator radial integral. For nuclei between $Z = 8$ and $Z = 84$, C ranges from about 30 to 40 MeV.

The rather good agreement, within the limited accuracy of both theory and experiment, furnishes more support for the essential validity of this calculation. Of course pairing correlations will modify the nuclear wave-functions somewhat[41] but will probably not affect the calculated moments greatly.

Table 3. Comparison between theoretical and experimental μ_N

Nucleus	Proton configuration	Neutron configuration (zeroth order)	Excitation mode of neutron	μ_N(calc)(nm) Schmidt limit	C=30 MeV	C=40 MeV	$\lvert\mu_N\rvert$(expt)(nm)
Ce^{137m}	$(1g_{7/2})^8$	$(2d_{5/2})^6(2d_{3/2})^4(1h_{11/2})^{11}$	$(1h_{11/2})^{11} \longrightarrow (1h_{11/2})^{10}(1h_{9/2})^1$	-1.91	-1.14	-1.01	0.96 ± 0.09
Ce^{137m}	$(1g_{7/2})^8$	$(2d_{5/2})^6(2d_{3/2})^4(3s_{1/2})^2(1h_{11/2})^9$	$(1h_{11/2})^9 \longrightarrow (1h_{11/2})^8(1h_{9/2})^1$	-1.91	-1.29	-1.19	
Ce^{137}	$(1g_{7/2})^8$	$(2d_{5/2})^6(2d_{3/2})^3(1h_{11/2})^{12}$	$(1h_{11/2})^{12} \longrightarrow (1h_{11/2})^{11}(1h_{9/2})^1$	+1.15	+0.97	+0.94	0.90 ± 0.15
Ce^{137}	$(1g_{7/2})^8$	$(2d_{5/2})^6(2d_{3/2})^1(3s_{1/2})^2(1h_{11/2})^{12}$	$(2d_{5/2})^6(2d_{3/2})^1 \longrightarrow (2d_{5/2})^5(2d_{3/2})^2$	+1.15	+0.82	+0.78	
Ce^{139}	$(1g_{7/2})^8$	$(2d_{5/2})^6(2d_{3/2})^3(3s_{1/2})^2(1h_{11/2})^{12}$	$(1h_{11/2})^{12} \longrightarrow (1h_{11/2})^{11}(1h_{9/2})^1$	+1.15	+0.97	+0.94	0.95 ± .20
Ce^{141}	$(1g_{7/2})^8$	$(1h_{11/2})^{12}(2f_{7/2})^1$	$(1h_{11/2})^{12} \longrightarrow (1h_{11/2})^{11}(1h_{9/2})^1$	-1.91	-1.48	-1.41	1.30 ± .20
Ce^{143}	$(1g_{7/2})^8$	$(1h_{11/2})^{12}(2f_{7/2})^3$	$(1h_{11/2})^{12}(2f_{7/2})^3 \longrightarrow (1h_{11/2})^{11}(1h_{9/2})^1(2f_{7/2})^2(2f_{5/2})^1$	-1.91	-1.21	-1.10	1.0 ± 0.3
Ce^{143}	$(1g_{7/2})^8$	$(1h_{11/2})^{12}(1h_{9/2})^2(2f_{7/2})^1$	$(1h_{11/2})^{12}(1h_{9/2})^2 \longrightarrow (1h_{11/2})^{11}(1h_{9/2})^3$	-1.91	-1.58	-1.51	

ACKNOWLEDGMENTS

We gladly acknowledge the suggestions of Professor John O. Rasmussen. We wish to thank Mrs. Mab I. Tocher for providing the ethylsulfate crystals, and Mr. Michiyuki Nakamura for his assistance in designing the polarimeter. We are grateful to the crew of thw ORNL cyclotron and the crew of the Livermore LRL reactor for carrying out the bombardments for these experiments.

FOOTNOTES AND REFERENCES

*Work performed under the auspices of the U.S. Atomic Energy Commission.

†Present address: Laboratoire Joliot-Curie De Physique Nucleaire, Universite de Paris, Orsay, France.

1. H. Noya, A. Arima, and H. Horie, Progr. Theoret. Phys. (Kyoto) 12, 623 (1955).
2. J. N. Haag, C. E. Johnson, D. A. Shirley, and D. H. Templeton, Phys. Rev. 121, 591 (1961).
3. A. Y. Cabezas, Electronic and Nuclear Properties of Some Radioactive Rare-Earth Elements (Thesis), Lawrence Radiation Laboratory Report UCRL-9346, 1960.
4. R. W. Kedzie, M. Abraham, and C. D. Jeffries, Phys. Rev. 108, 54 (1957).
5. L. E. Glendenin, Anal. Chem. 27, 50 (1955).
6. C. F. M. Cacho, M. A. Grace, C. E. Johnson, A. K. Knipper, R. G. Scurlock, and R. T. Taylor, Phil. Mag. 46, 1287 (1955).
7. E. Ambler, R. P. Hudson, and G. M. Temmer, Phys. Rev. 97, 1212 (1955).
8. H. Meyer, Phil. Mag. 2, 521 (1957).
9. J. M. Daniels and F. N. H. Robinson, Phil. Mag. 4, 630 (1953).
10. M. E. Rose, Phys. Rev. 91, 610 (1953).
11. F. Metzger and M. Deutsch, Phys. Rev. 78, 551 (1950).
12. R. J. Blin-Stoyle and M. A. Grace, in Handbuch der Physik, Vol. 42, p. 555 (Springer-Verlag, Berlin, 1957).
13. O. Klein and Y. Nishina, Z. Physik 52, 853 (1929).
14. This equation differs from Eq. (12.15) of Ref. 12 in that our F parameters are normalized by $1/(1+\delta^2)$.

15. K. W. H. Stevens, Proc. Phys. Soc. (London) A65, 209 (1952).

16. R. J. Elliott and K. W. H. Stevens, Proc. Roy. Soc. (London) A215, 437 (1952); 218, 553 (1953); 219, 387 (1953).

17. B. R. Judd and I. Lindgren, Phys. Rev. 122, 1802 (1961).

18. H. Kopfermann, Nuclear Moments (Academic Press, Inc., New York, 1958) p. 398.

19. A. R. Brosi and B. H. Ketelle, Phys. Rev. 100, 169 (1955); 103, 917 (1956).

20. E. Ambler, R. P. Hudson, and G. N. Temmer, Phys. Rev. 101, 196 (1956).

21. G. T. Danby, J. S. Foster, and A. L. Thompson, Canadian Journal of Physics 36, 1487 (1958).

22. S. A. Moszkowski, in "Beta-and Gamma-Ray Spectroscopy", edited by Kai Siegbahn (Interscience, 1955).

23. B. H. Ketelle, H. Thomas, and A. R. Brosi, Phys. Rev. 103, 190 (1956).

24. J. E. Mack, Revs. Modern Phys. 22, 64 (1950).

25. T. R. Gerholm and H. deWaard, Physica 21, 601 (1955).

26. B. S. Dzhelepov, B. K. Preobrazhenskii, I. M. Ragachev, and P. A. Tishken, Bull. Acad. Sci. USSR 22, 923 (1958).

27. K. Kotajima and H. Morinaga, Nuclear Phys. 16, 231 (1960).

28. W. H. Kelly, G. B. Beard, W. B. Chaffee, and J. M. Gonser, Nuclear Phys. 19, 79 (1960).

29. N. P. Heydenberg and G. M. Temmer, Phys. Rev. 100, 150 (1955).

30. J. G. V. Taylor and Janet S. Merritt, Bull. Amer. Phys. Soc., Series II, Vol. 7, p. 352 (1962).

31. D. Strominger, J. M. Hollander, and G. T. Seaborg, Revs. Modern Phys. 30, 585 (1958).

32. H. L. Polak, W. Schoo, B. L. Schram, R. K. Girgis, and R. van Lieshout, Nuclear Phys. 5, 271 (1958).

33. M. C. Joshi, B. N. Subba Rao, and B. V. Thosar, Nuovo Cimento 9, 600 (1958).

34. H. deWaard and T. R. Gerholm, Physica 21, 599 (1955); Nuclear Phys. 1, 281 (1956).

35. J. R. Cook, Proc. Phys. Soc. (London) 77, 346 (1961).

36. L. A. Sliv and I. M. Band, University of Illinois Trans. Report 571CCK1, Physics Dept. Urbana, 1956.

37. S. H. Vegors, R. L. Heath, and W. Hammer, Graphs of the K-Conversion Coefficients as Calculated by Sliv and Band, Aug. 1959 (privately distributed).

38. R. C. Sapp and W. W. Strohm, Jr., Department of Physics, University of Kansas, private communication (July, 1962).

39. D. W. Martin, M. K. Brice, J. M. Cork, and S. B. Burson, Phys. Rev. 101, 182 (1956).

40. Richard Marrus, Lawrence Radiation Laboratory, private communication.

41. N. Freed and L. S. Kisslinger, Nuclear Physics 25, 611 (1961).

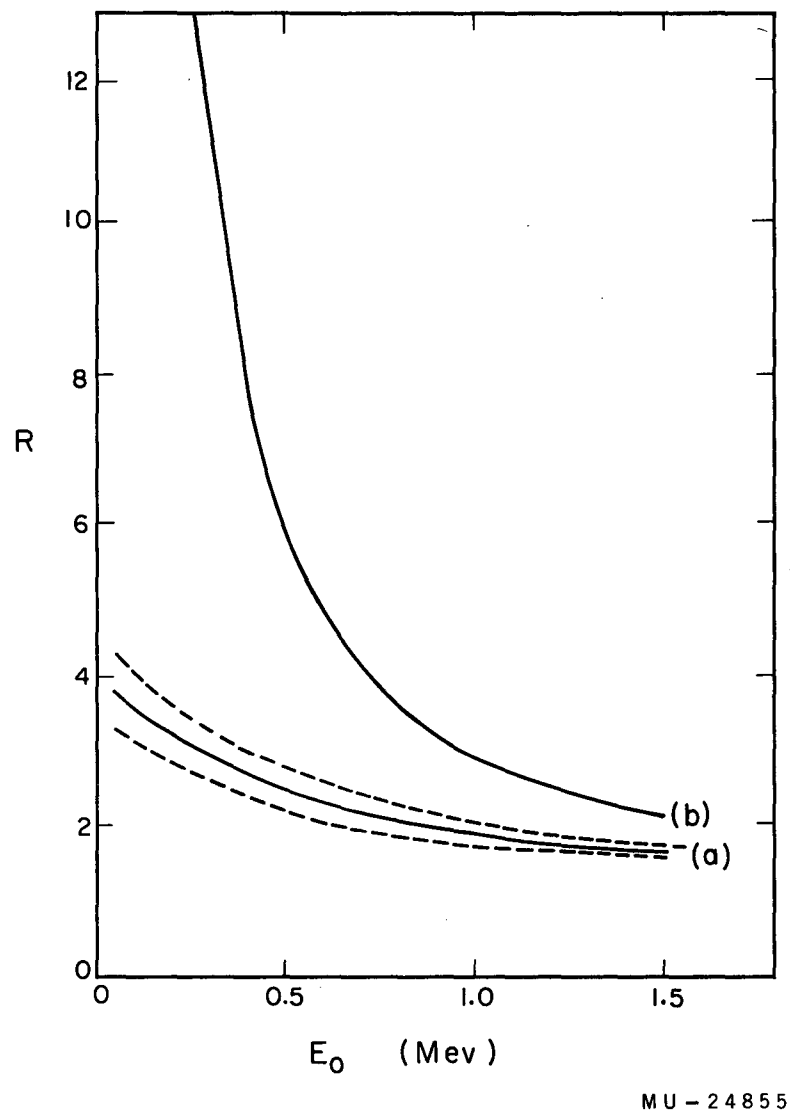

Fig. 1. The parameter R as a function of incident γ-ray energy. The solid curve (a) is for $\delta=80^\circ$, $\Delta\delta=\Delta\eta=70^\circ$. The upper (lower) dashed curve is for $\delta=80^\circ$, $\Delta\delta=\Delta\eta=63^\circ$ (77°). The solid curve (b) is for $\delta=80^\circ$, $\Delta\delta=\Delta\eta=0^\circ$.

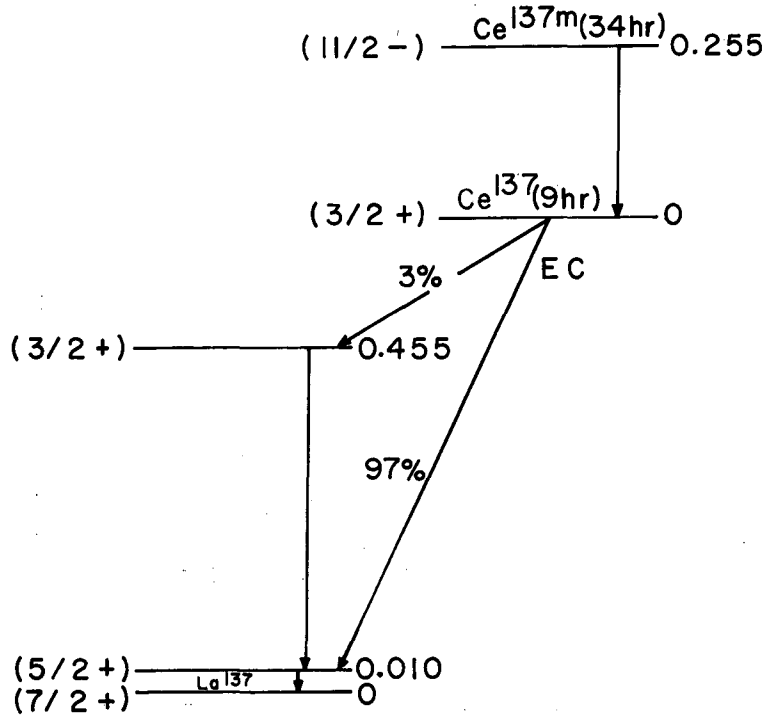

Fig. 2. The decay scheme of Ce^{137m} and Ce^{137}.

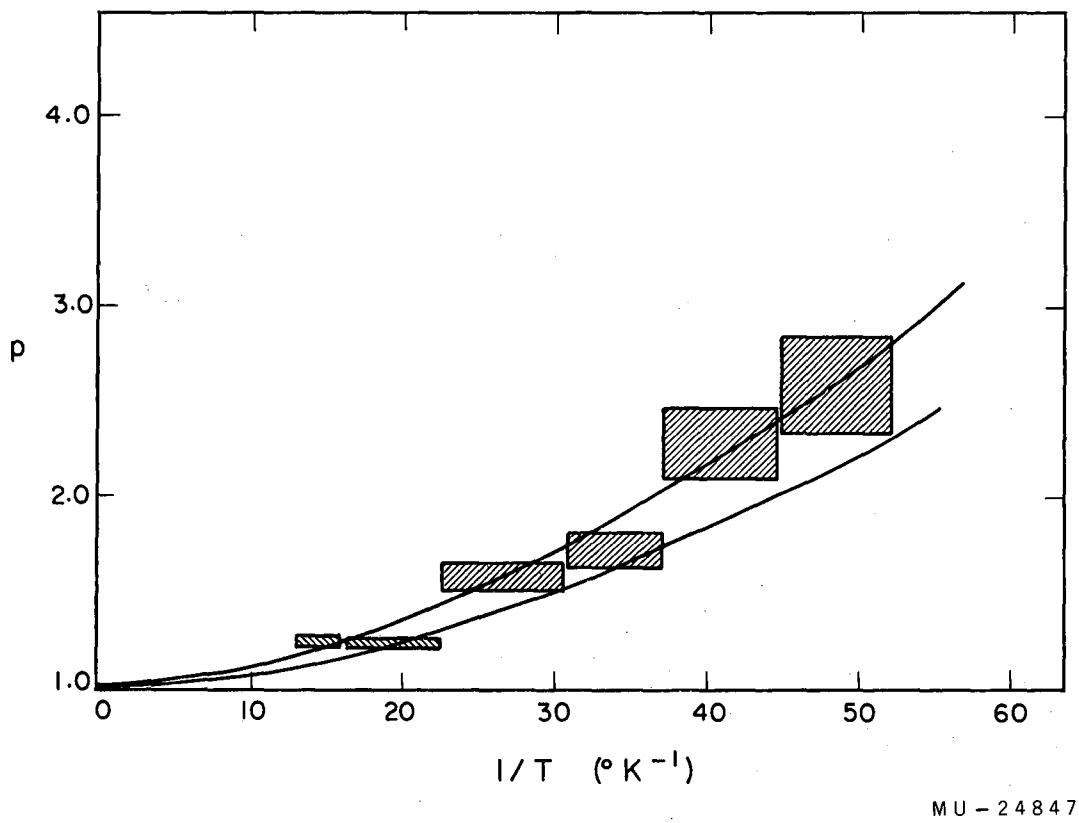

Fig. 3. Linear polarization of the 255-keV γ-ray from Ce^{137m} in NES. For clarity the experimental points in each temperature range have been averaged: the shaded area denotes the temperature range and the total error in p.

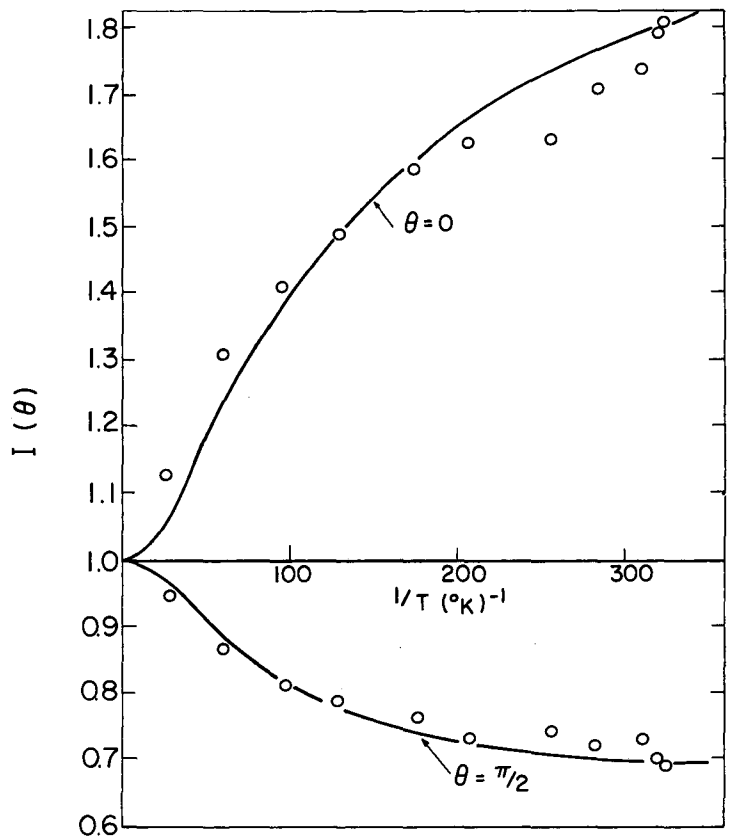

MU-26859

Fig. 4. Intensity of the 255 keV γ-ray from Ce^{137m} oriented in CMN, as a function of reciprocal temperature. The theoretical curves are for $|\mu_N| = 0.92$ nm.

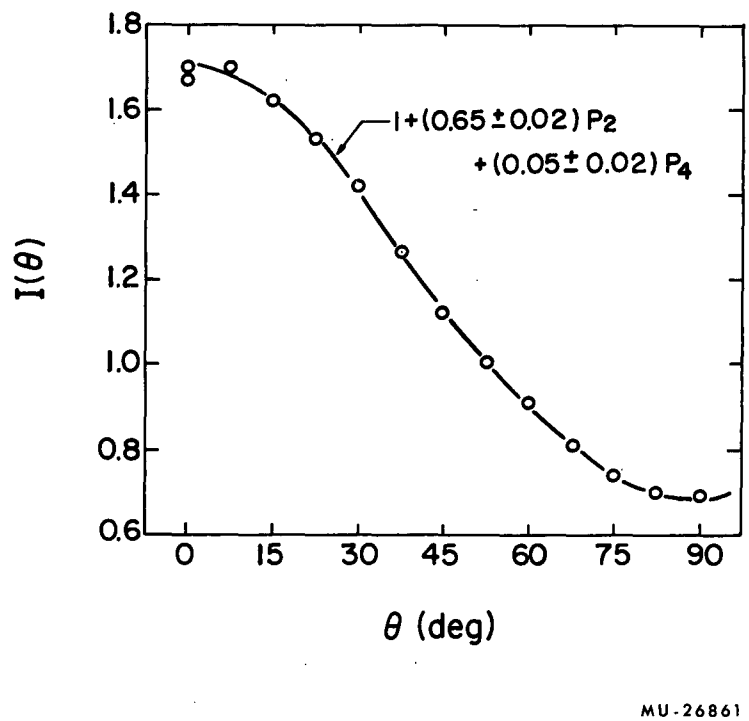

Fig. 5. Angular distribution of the 255 keV γ-ray from Ce^{137m} in CMN, at .0043°K. The curve shown was fitted to the data. The theoretical curve, based on μ_N=0.92 and the decay scheme in Fig. 2, is $1+0.63\ P_2 + 0.07\ P_4$.

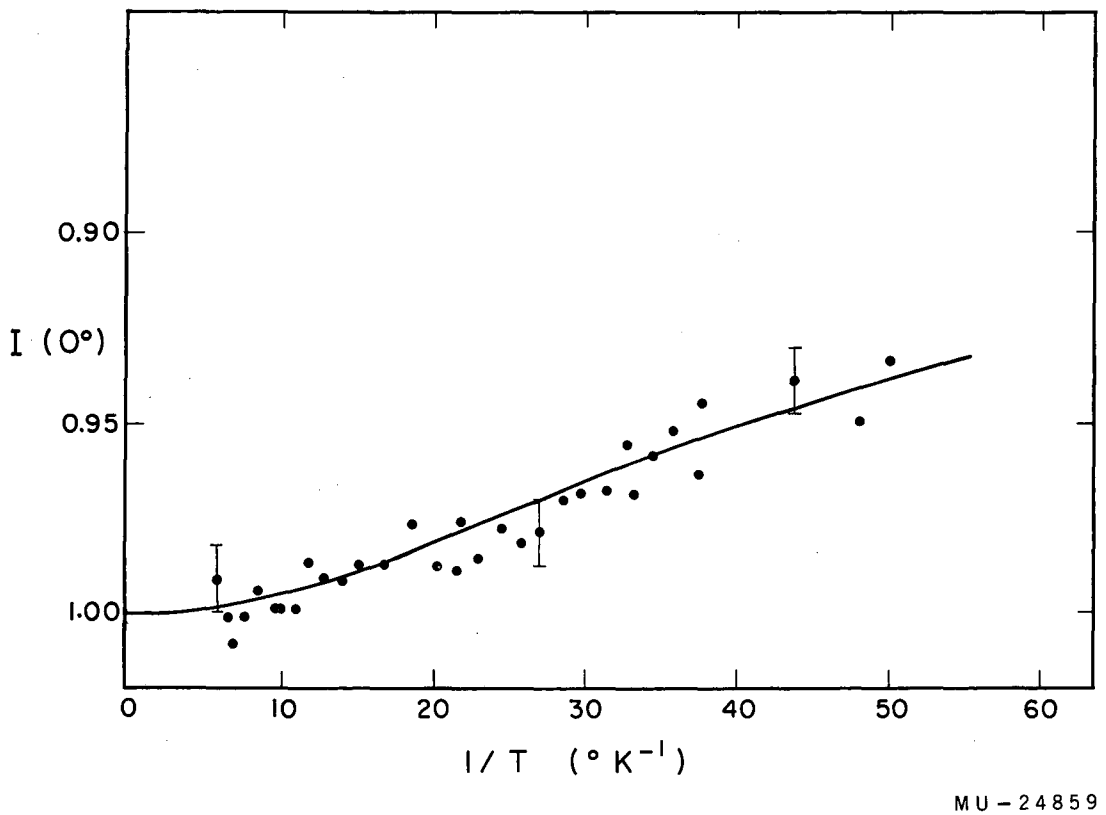

Fig. 6. Intensity along the crystalline axis of the 445 keV γ-ray of La^{137} following the decay of Ce^{137} oriented in NES, as a function of temperature.

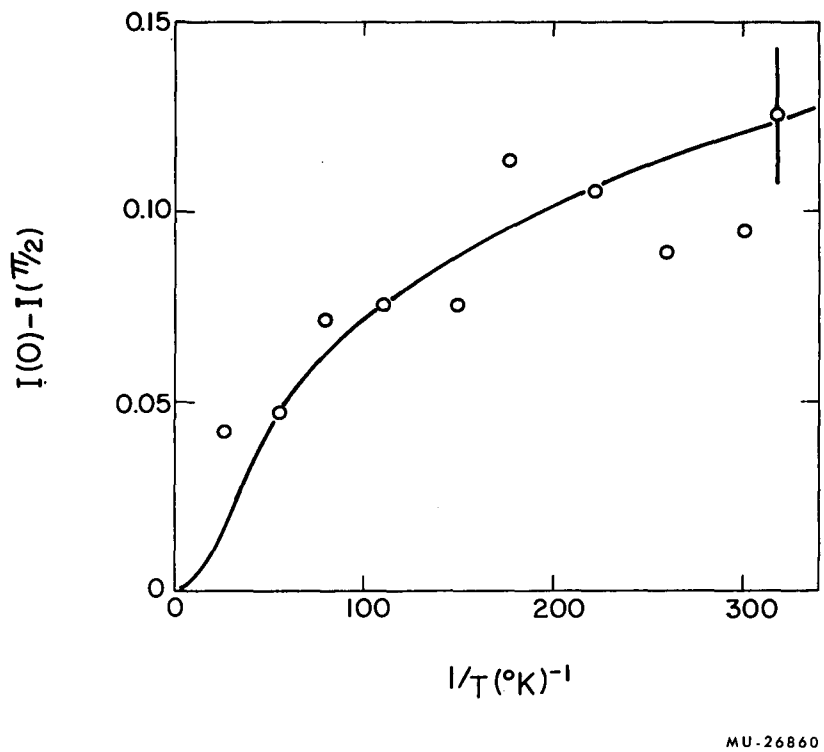

Fig. 7. Difference between the intensities along and perpendicular to the c axis of the 445 keV γ-ray of La^{137} following the decay of Ce^{137} oriented in CMN, plotted against reciprocal temperature.

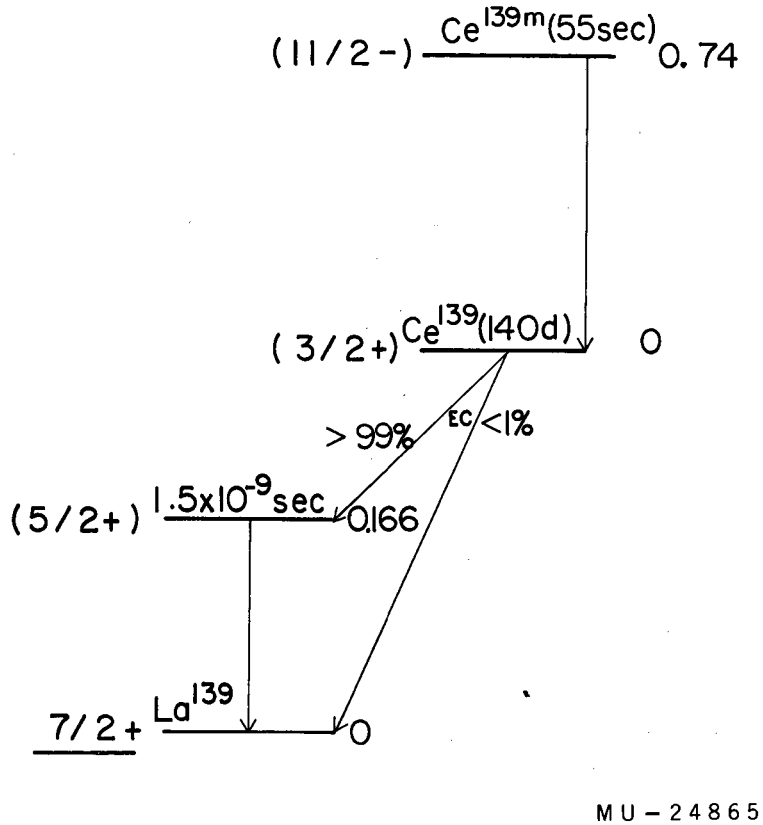

Fig. 8. Decay scheme of Ce^{139}.

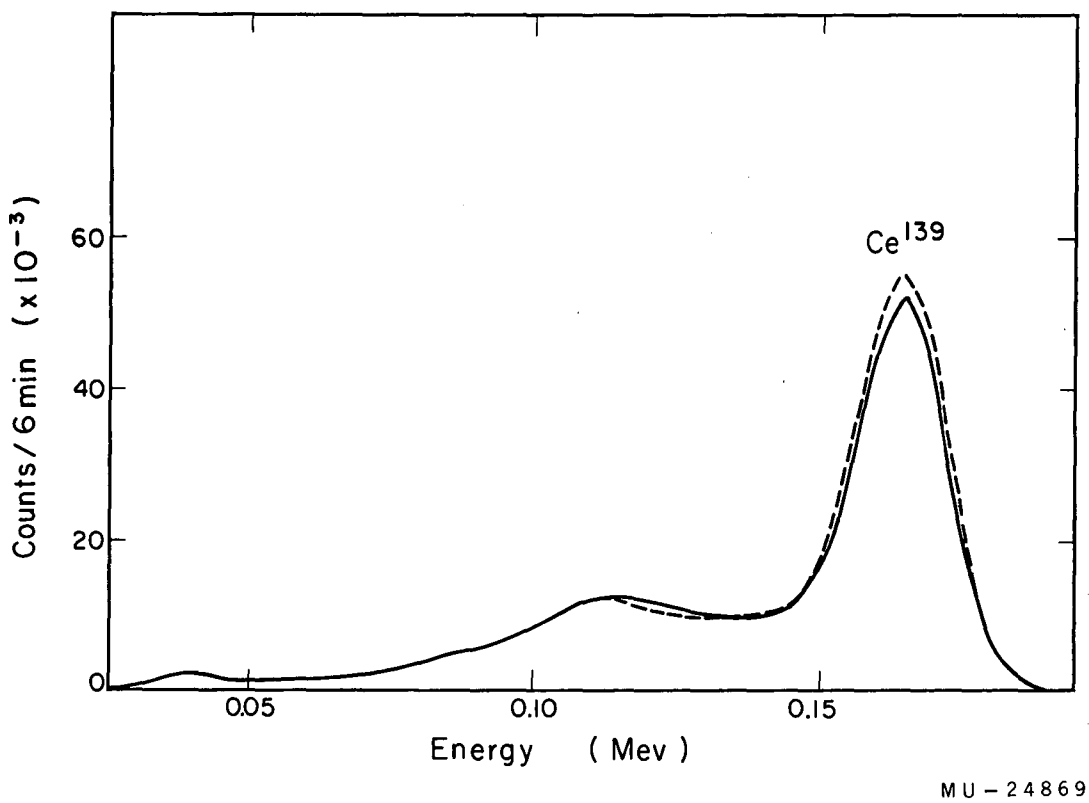

Fig. 9. Gamma ray spectrum from La^{139} following the decay of Ce^{139} in an NES lattice, taken along the crystal axis. The dashed curve represents the spectrum at 0.02°K, the solid curve that at 1.3°K. Note that the anisotropy on the Compton peak is opposite to that in the photopeak, due to right-angle Compton scattering of the plane-polarized radiation at $\theta = 90°$.

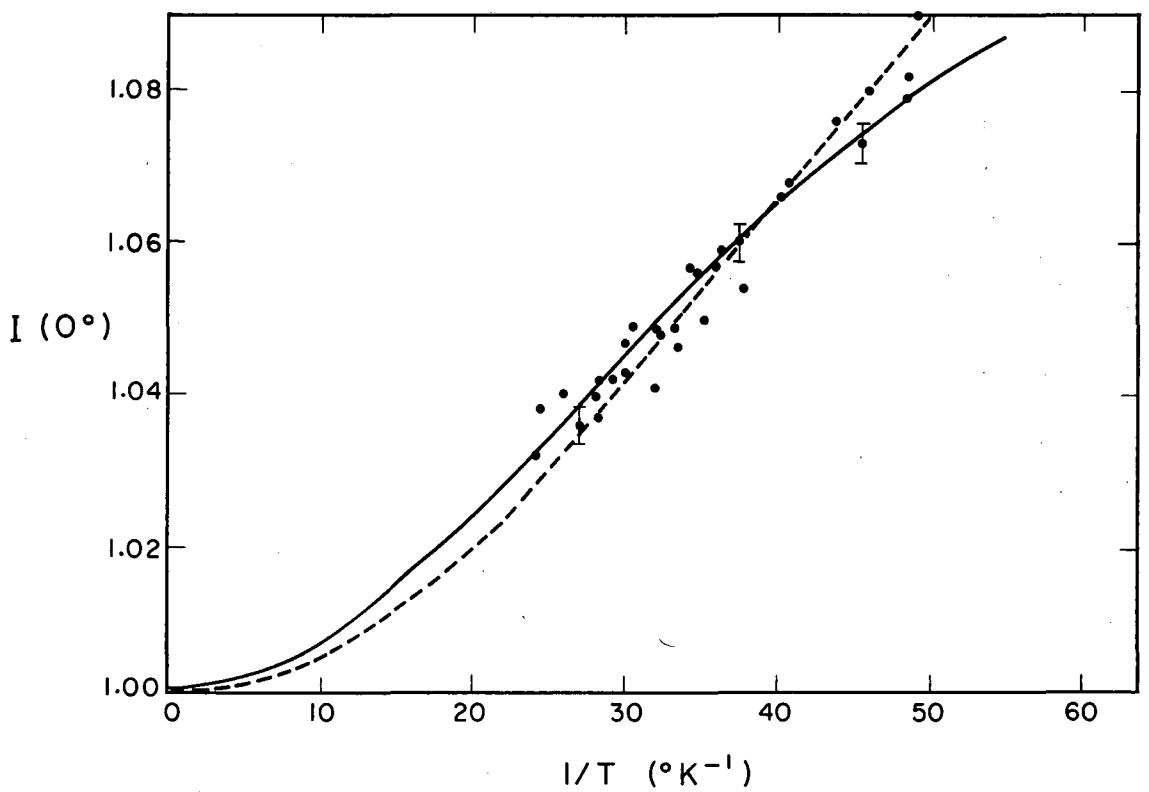

Fig. 10. Intensity of the 168-keV γ-ray of La^{139} following the decay of Ce^{139} oriented in NES, along the crystalline c axis, as a function of reciprocal temperature.

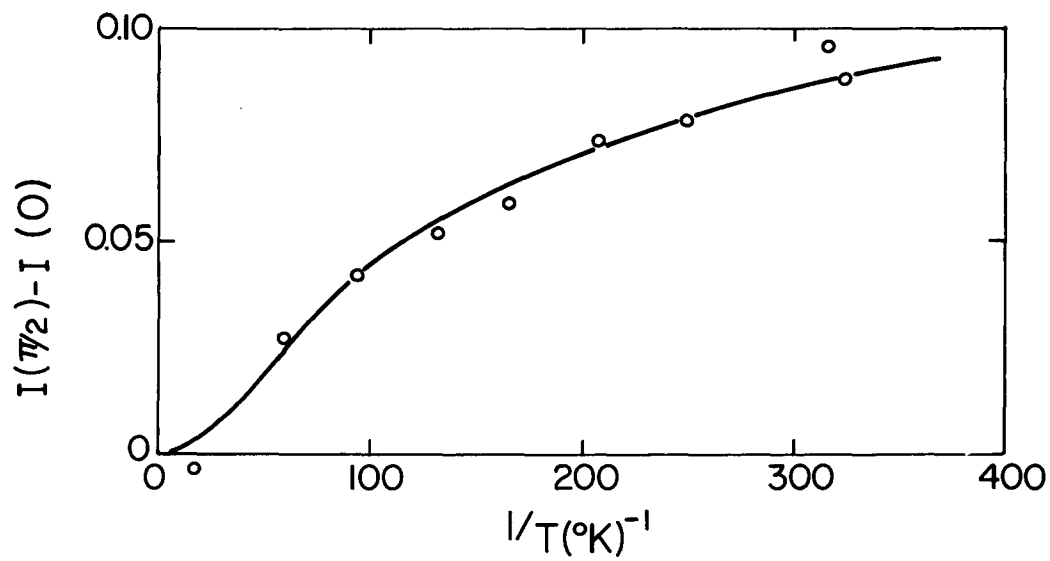

MU-26858

Fig. 11. Intensity difference, along and perpendicular to the axis, of the 166-keV γ-ray following the decay of Ce^{139} oriented in CMN, as a function of reciprocal temperature.

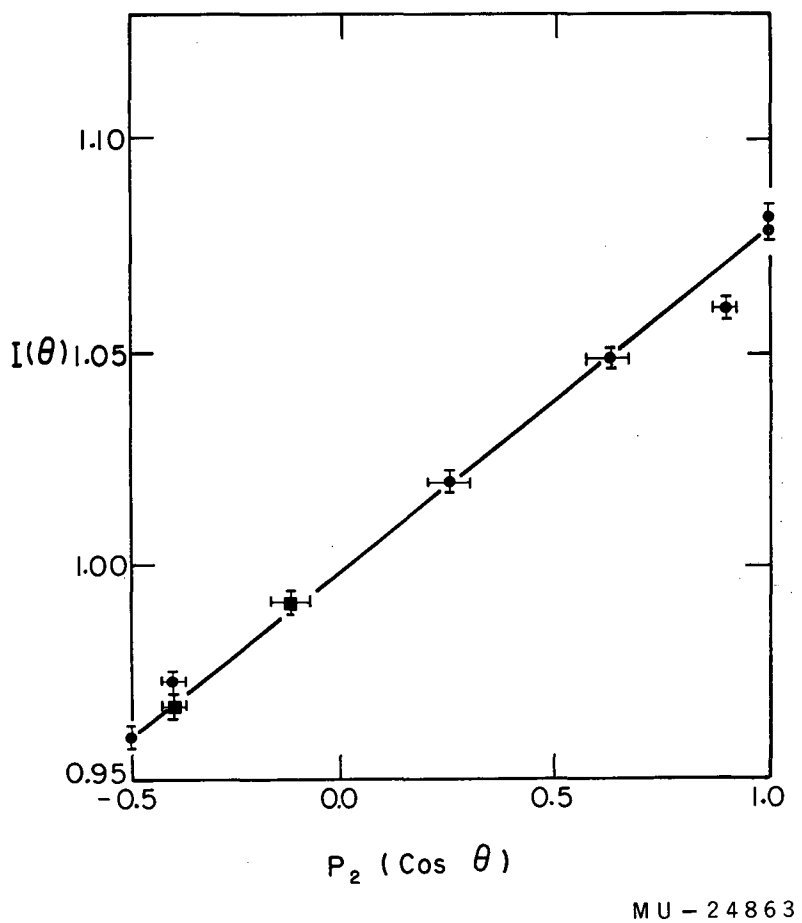

Fig. 12. Angular dependence of intensity of the 166 keV γ-ray following the decay of Ce^{139} in NES at 0.02°K, plotted against $P_2(\cos\theta)$. The linear relationship indicates a pure P_2 dependence.

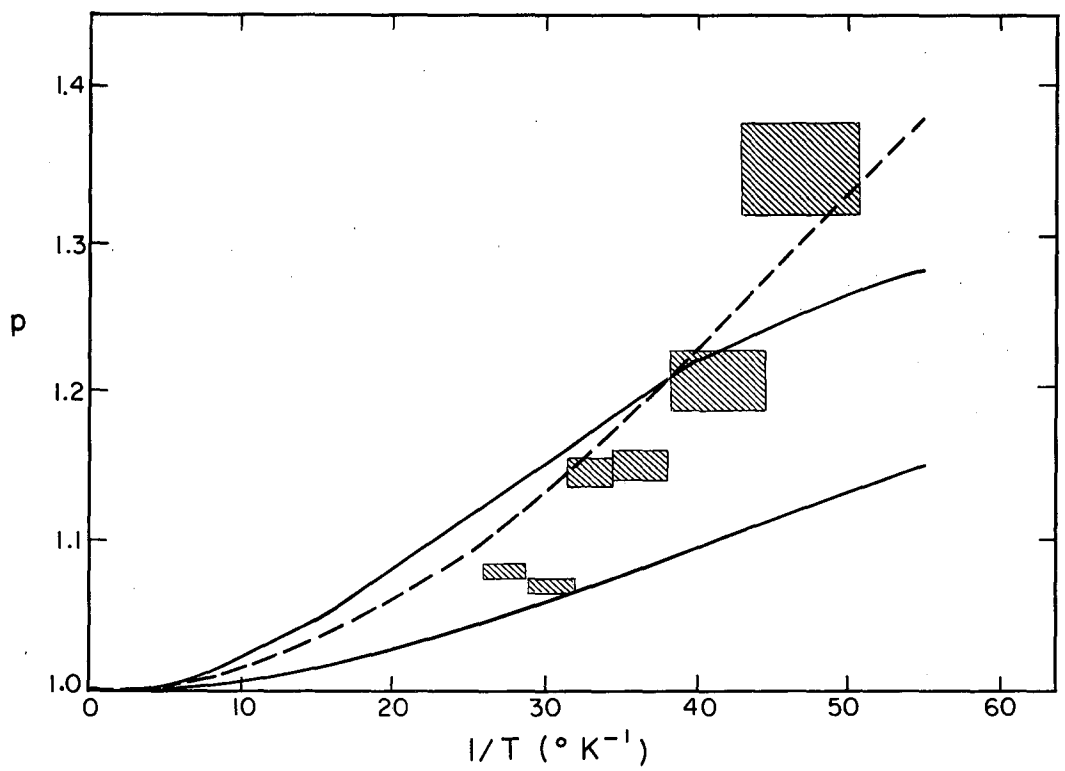

MU-24851

Fig. 13. Temperature dependence of linear polarization of the 166-keV γ-ray following the decay of Ce^{139} oriented in NES. The solid theoretical curves are for predominantly dipole radiation and μ_N=1.15 nm (upper) and μ_N=0.75 nm (lower). The dashed curve is for a pure quadrupole transition with μ_N=0.6 nm.

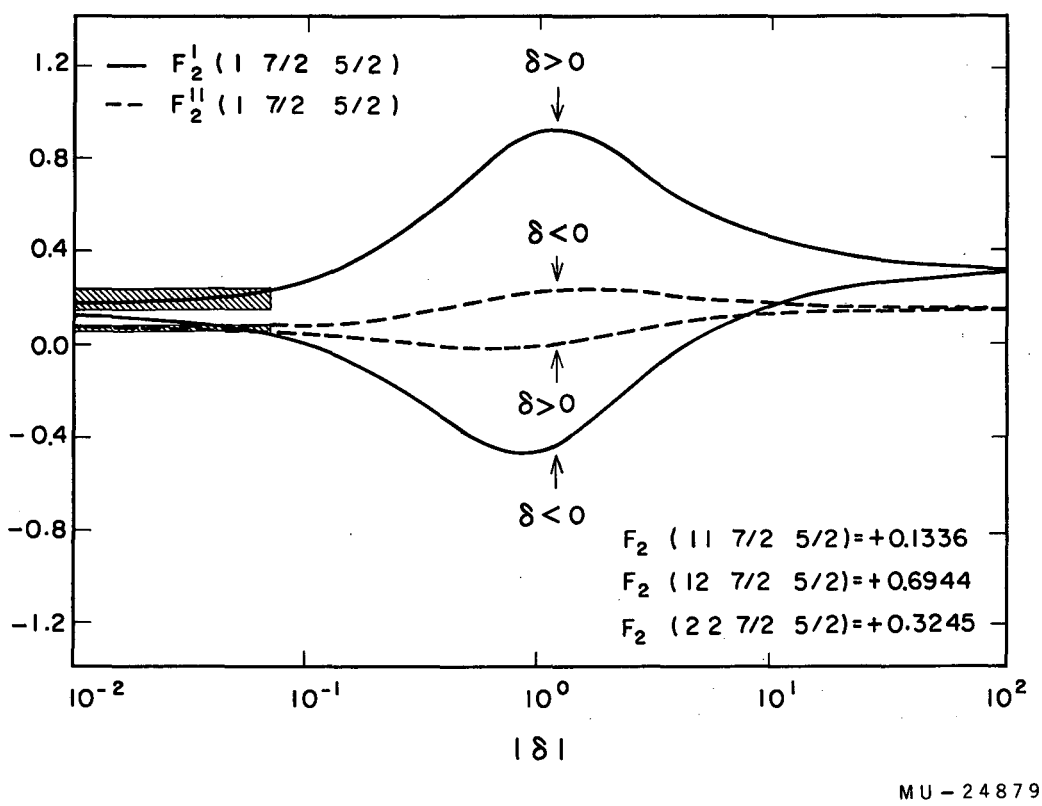

Fig. 14. Theoretical F coefficients vs. amplitude mixing ratio for a 5/2 (M1,E2)7/2 transition. Shaded areas fit experimental results for Ce^{139} in NES.

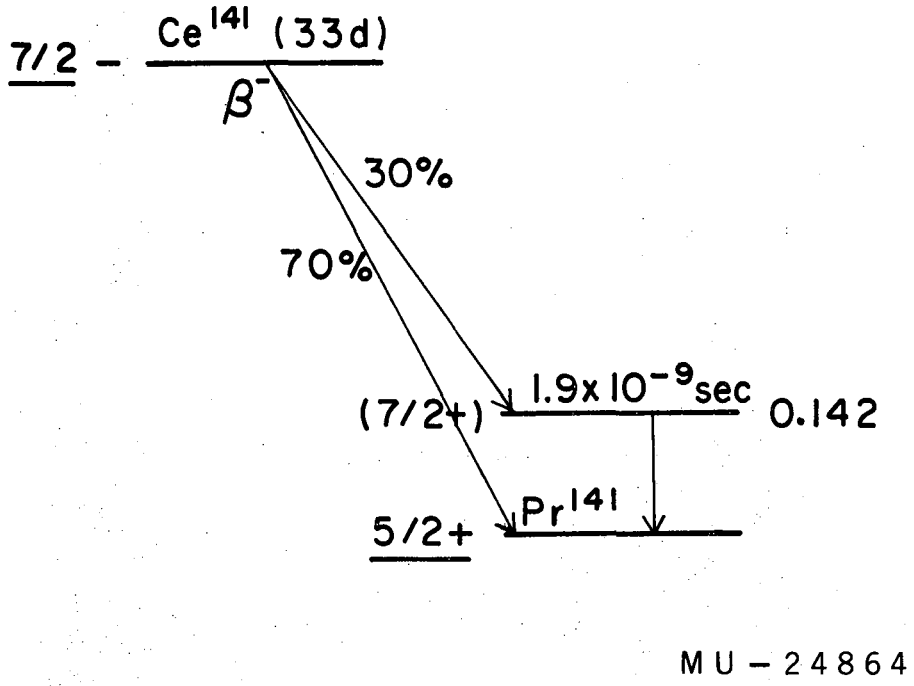

Fig. 15. Decay scheme of Ce^{141}.

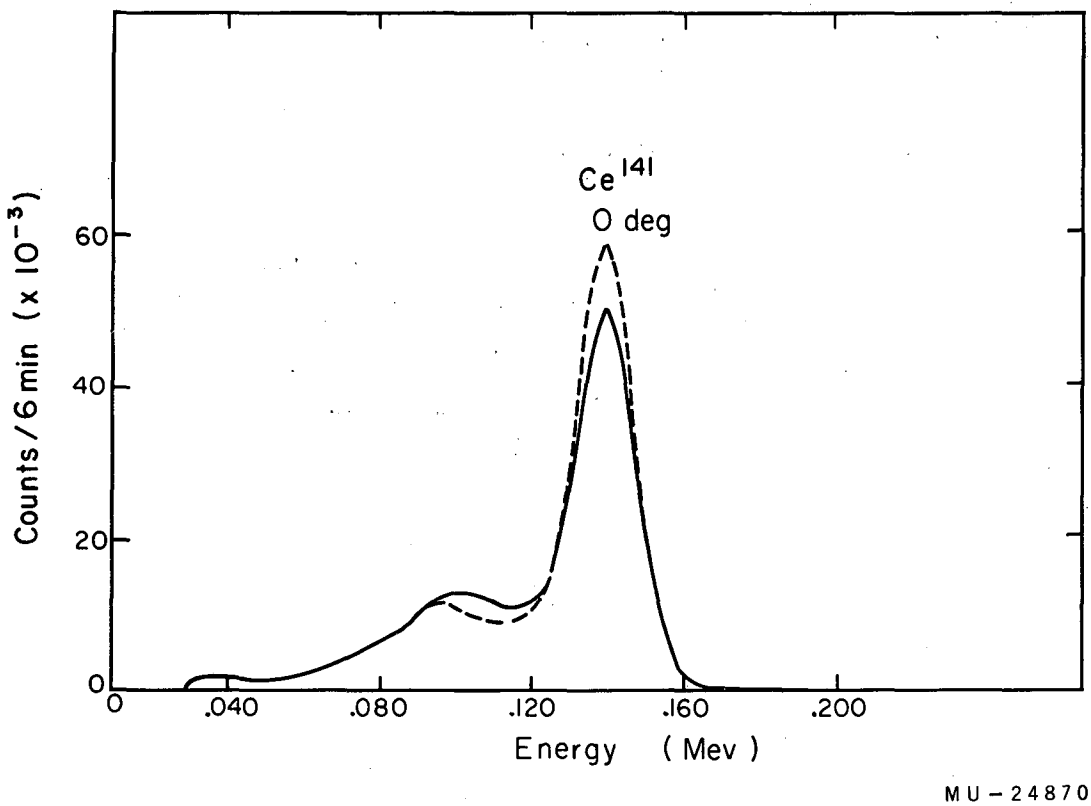

Fig. 16. Gamma ray spectrum from Ce^{141} oriented in NES, taken along the crystal axis. The solid curve was obtained with the source at 1.3°K, the dashed curve with the source at 0.02°K.

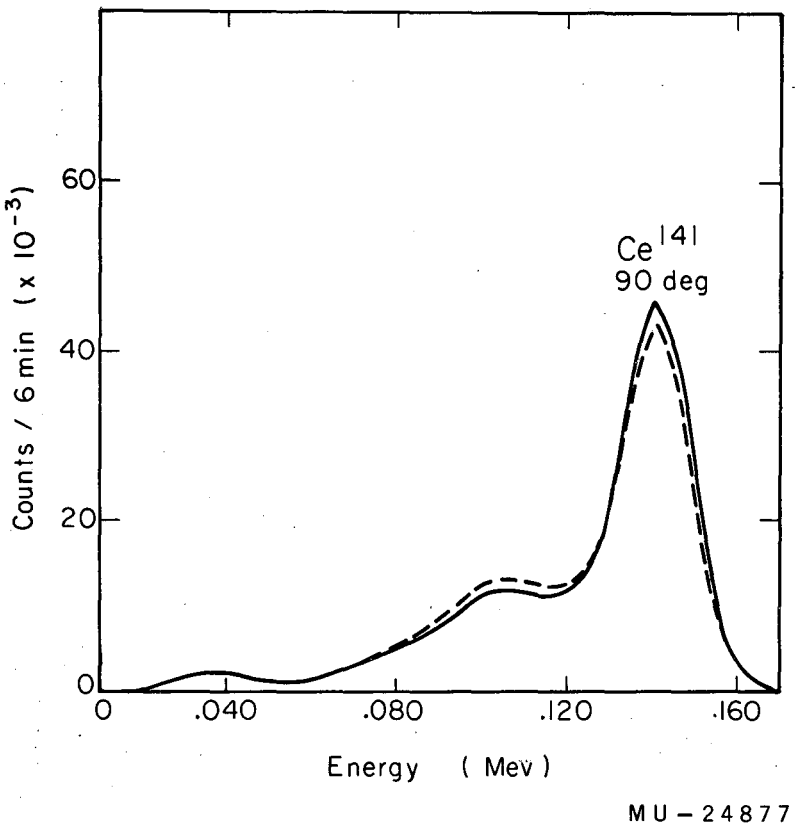

Fig. 17. Similar to Fig. 16, but at 90° from the crystalline c axis, Note the opposite anisotropy of the Compton peak, explained in text.

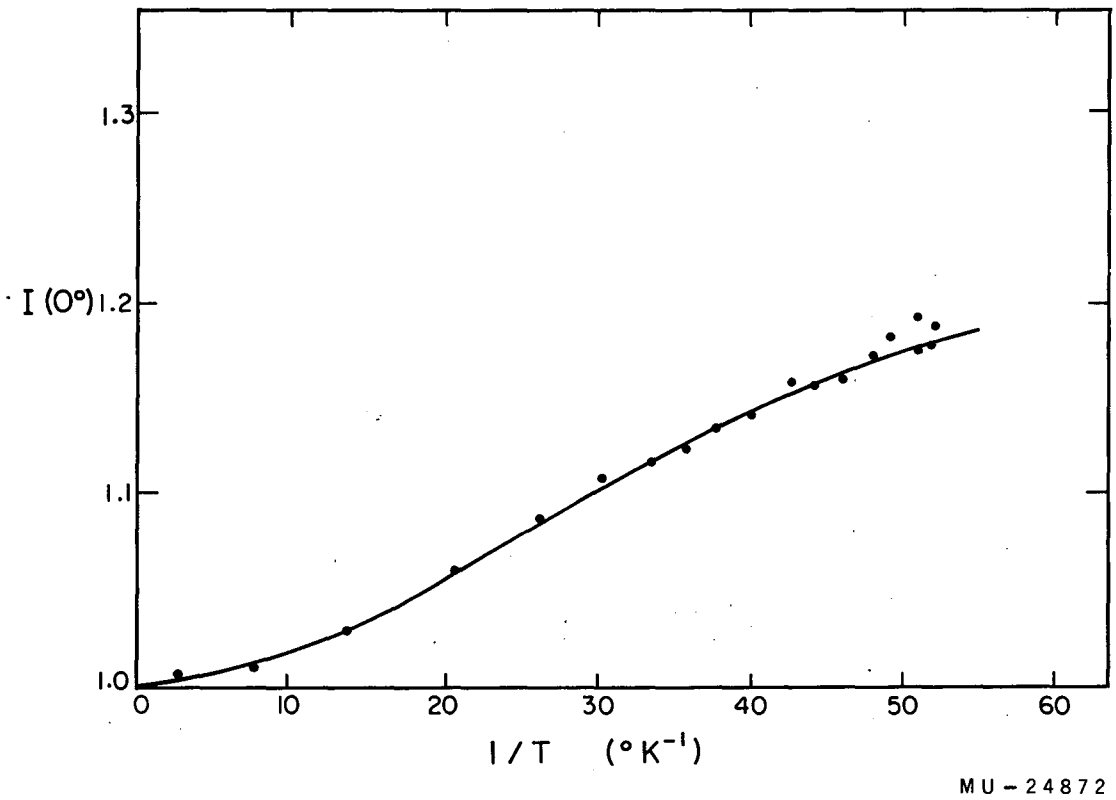

Fig. 18. Intensity along the c axis of the 142 keV γ-ray of Pr^{141} following the decay of Ce^{141} oriented in NES, as a function of temperature. The theoretical curve is for μ_N=1.3 nm.

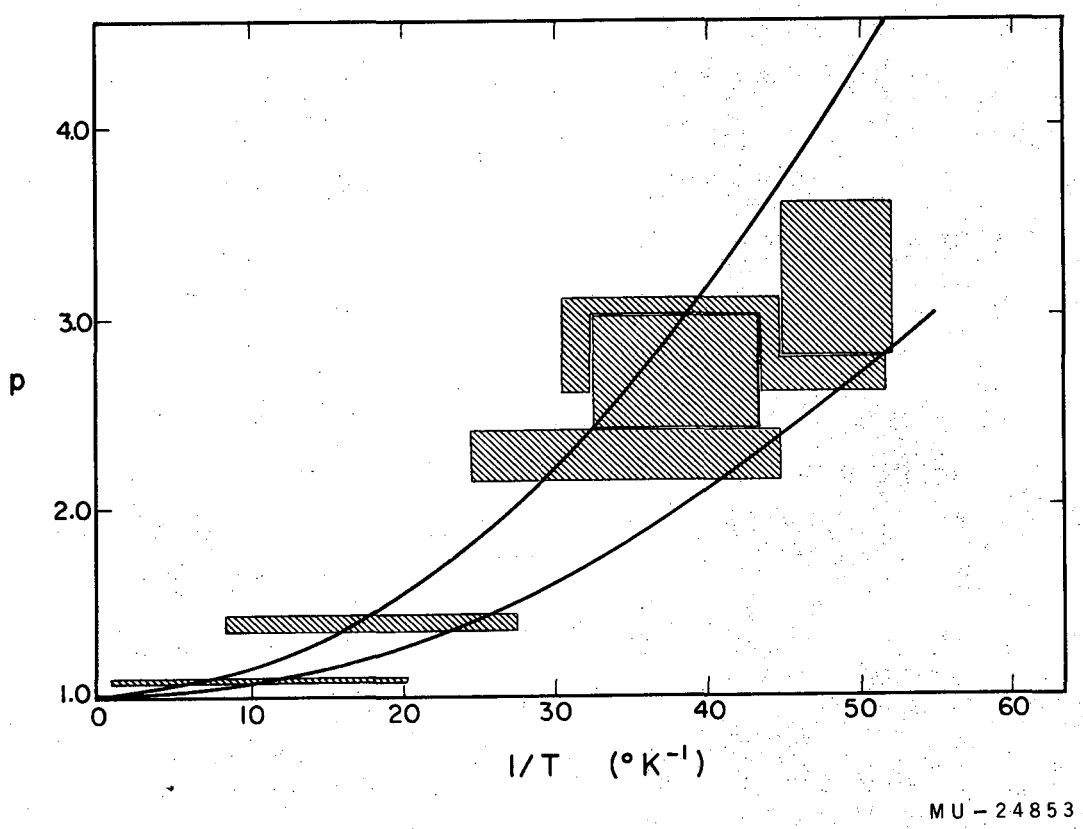

Fig. 19. Temperature dependence of polarization of the 142 keV γ-ray following the decay of Ce^{141} oriented in NES. The theoretical curves are for nuclear moments (for Ce^{141}) of 1.5 nm (upper) and 1.1 nm (lower). The shaded area represents the extent of the total limits of error in p (vertical) and the total temperature interval over which each measurement was taken. The actual experimental uncertainty in the average 1/T for each temperature is only about 3 units in 1/T, and the data could be represented by shaded areas of that width.

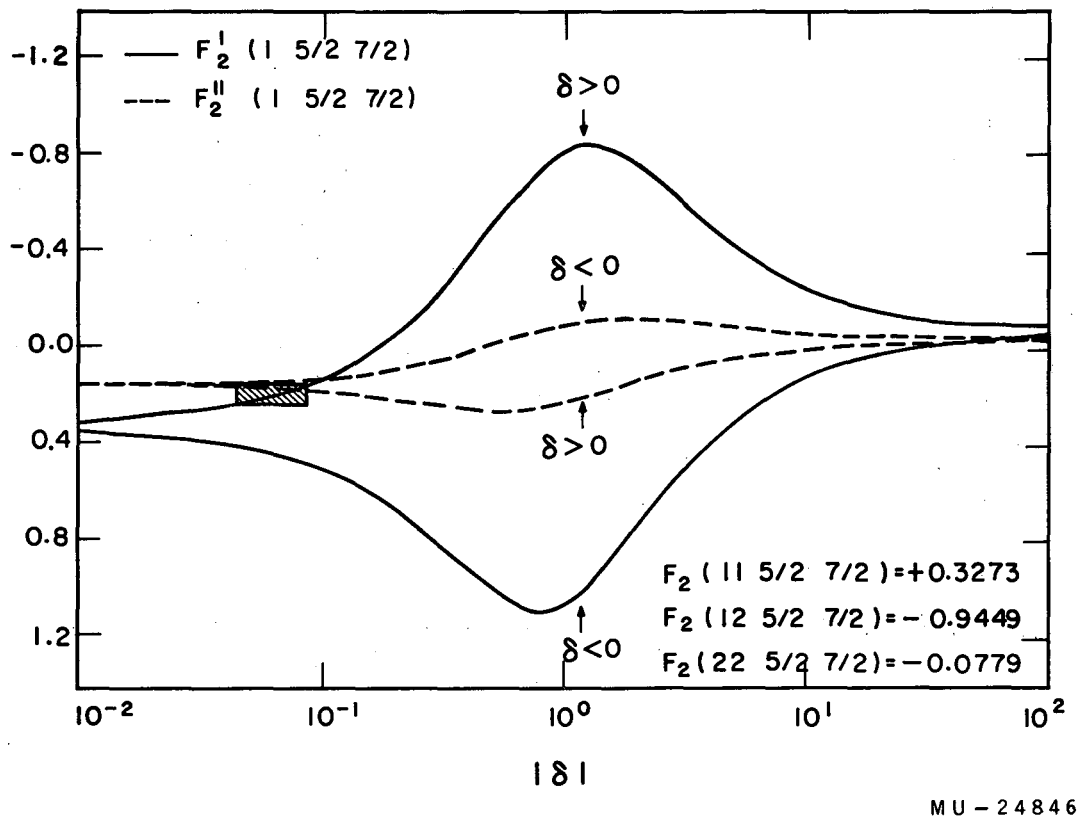

Fig. 20. Plot of the F parameters for the sequence 5/2 (M1,E2)7/2. The shaded area is allowed by our data for this sequence in Pr^{141}.

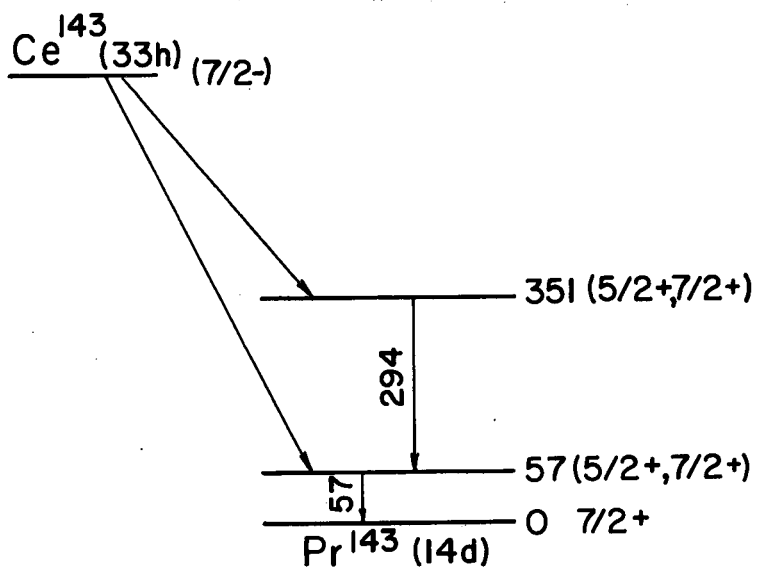

MU-26862

Fig. 21. Part of the decay scheme of Ce^{143}. Level sequences and energies are from Ref. 39. The spin of Pr^{143} is from Ref. 40. The other spins are tentatively assigned by us from this work and shell model systematics.

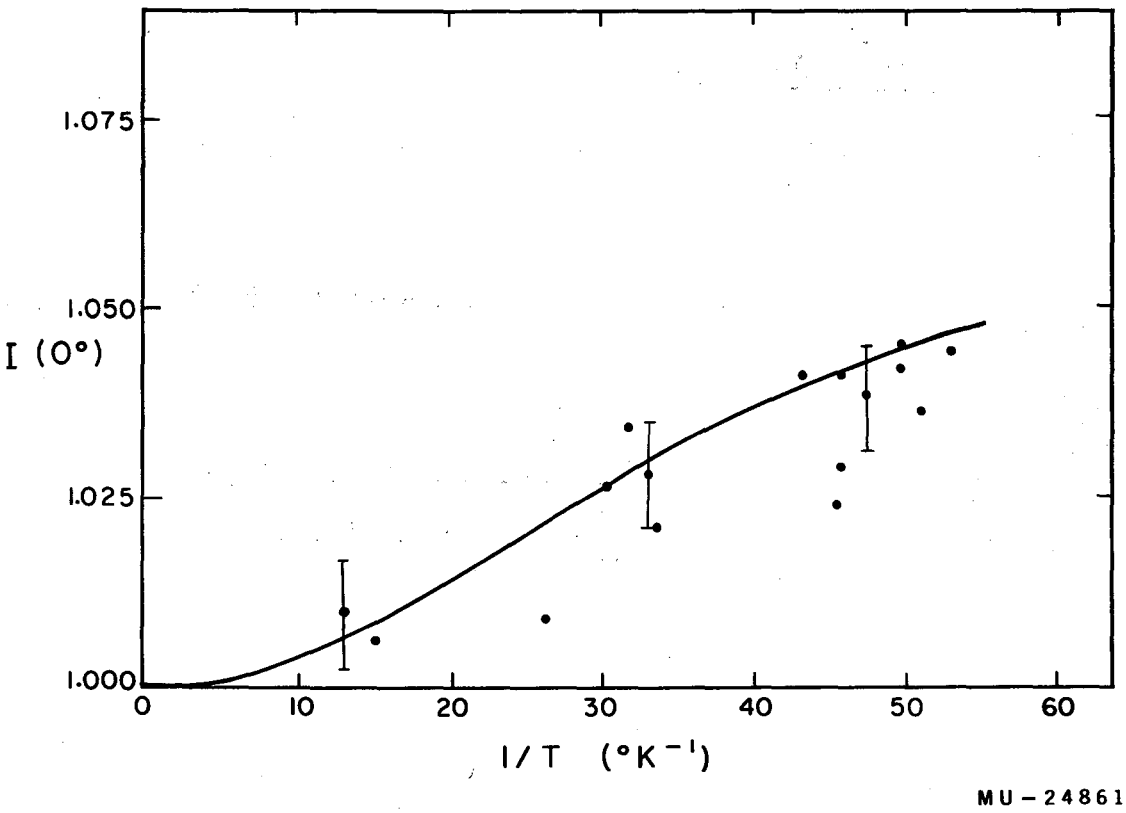

Fig. 22. Intensity along the c axis of the 294 keV γ-ray of Pr^{143} following the decay of Ce^{143} oriented in NES. The theoretical curve is for $\mu_N = 1$ nm.

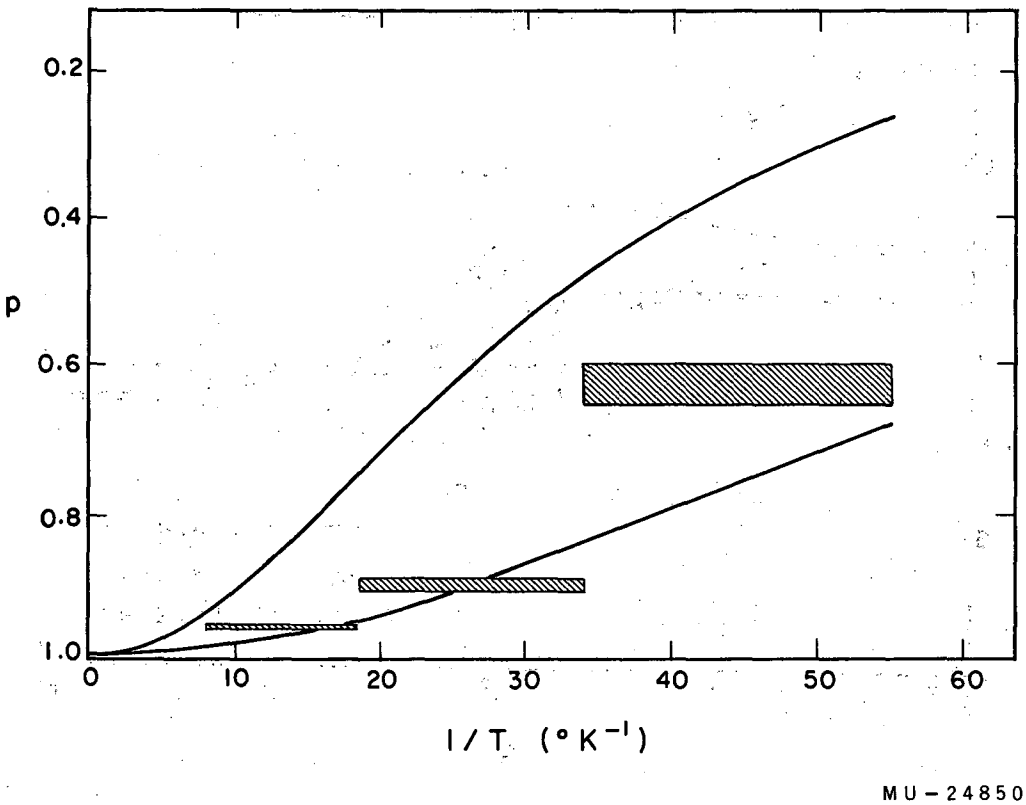

Fig. 23. Temperature dependence of linear polarization of the 294 keV γ-ray following the decay of Ce^{143} oriented in NES. The curves are based on $\delta(E2/M1) \approx -.8$ and $\mu_N=1.3$ (upper) and 0.7 (lower), with the initial (351 keV) and final (57 keV) states both having spin 5/2 or 7/2.

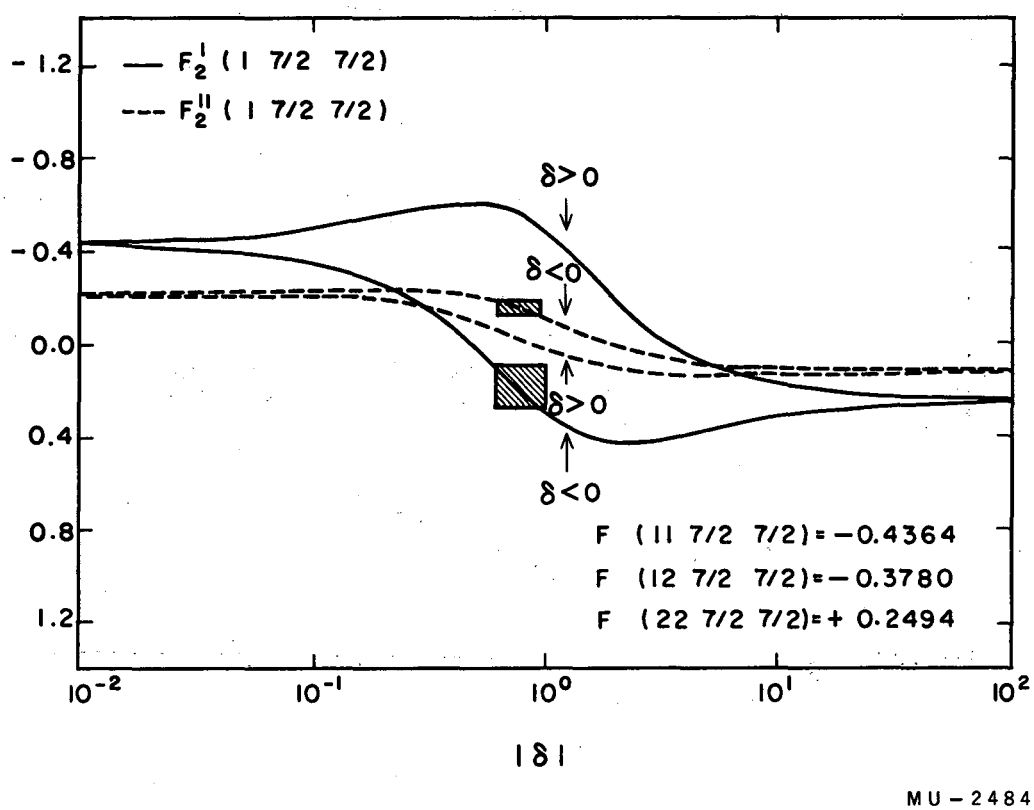

Fig. 24. The F parameters versus the amplitude mixing ratio for the sequence 7/2(M1,E2)7/2. The shaded areas give the range of allowed by these experiments for the 294 keV transition in Pr^{143}. As might be expected classically the sequence 5/2 (M1,E2)5/2 gives an "F-plot" almost identical to this one: in fact, this latter sequence fits the data equally well.

This report was prepared as an account of Government sponsored work. Neither the United States, nor the Commission, nor any person acting on behalf of the Commission:

A. Makes any warranty or representation, expressed or implied, with respect to the accuracy, completeness, or usefulness of the information contained in this report, or that the use of any information, apparatus, method, or process disclosed in this report may not infringe privately owned rights; or

B. Assumes any liabilities with respect to the use of, or for damages resulting from the use of any information, apparatus, method, or process disclosed in this report.
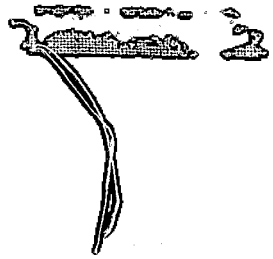
As used in the above, "person acting on behalf of the Commission" includes any employee or contractor of the Commission, or employee of such contractor, to the extent that such employee or contractor of the Commission, or employee of such contractor prepares, disseminates, or provides access to, any information pursuant to his employment or contract with the Commission, or his employment with such contractor.